Molecular Cell

Article

A Non-canonical PDK1-RSK Signal Diminishes Pro-caspase-8-Mediated Necroptosis Blockade

Graphical Abstract

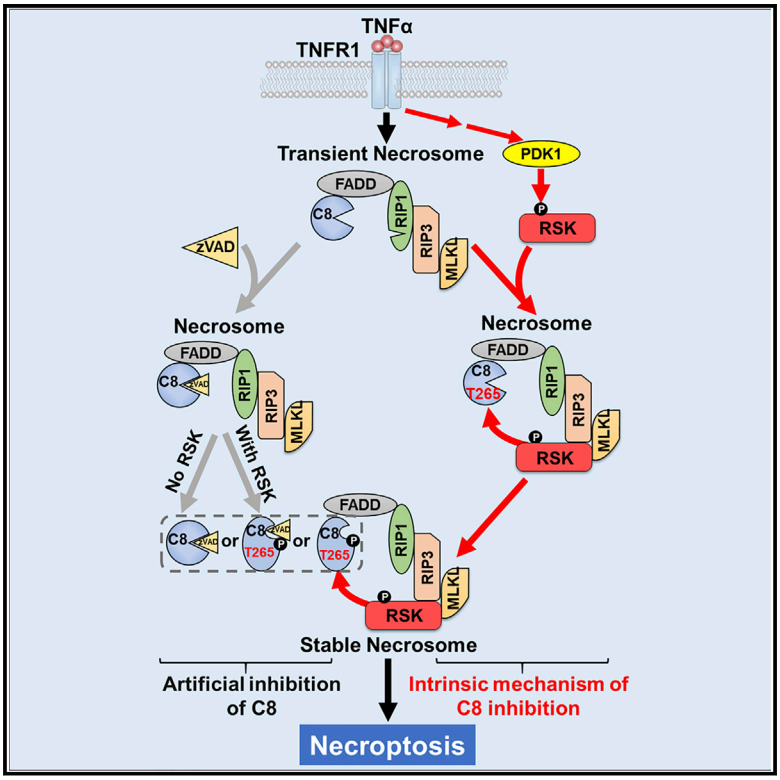

Authors

Zhang-Hua Yang, Xiao-Nan Wu, Peng He, ..., Zhi-Yu Cai, Wei Mo, Jiahuai Han

Correspondence

wmo@xmu.edu.cn (W.M.), jhan@xmu.edu.cn (J.H.)

In Brief

An intrinsic mechanism—RSK, activated by TNF via PDK1—for overcoming necroptosis blockade is revealed by Yang et al. that phosphorylates pro-caspase-8 at Thr265 within the necrosome to inactivate pro-caspase-8.

Highlights

- Phosphorylation of pro-caspase-8 at Thr265 releases the blockade of necroptosis
- RSK phosphorylates pro-caspase-8 at Thr265 in the necrosome
- PDK1 activates RSK by an ERK-independent mechanism to promote necroptosis
- RSK inhibition protects mice from TNF-induced cecum injury and lethality

Yang et al., 2020, Molecular Cell *80*, 1–15
October 15, 2020
https://doi.org/10.1016/j.molcel.2020.09.004

CellPress

Please cite this article in press as: Yang et al., A Non-canonical PDK1-RSK Signal Diminishes Pro-caspase-8-Mediated Necroptosis Blockade, Molecular Cell (2020), https://doi.org/10.1016/j.molcel.2020.09.004

Molecular Cell

CellPress

Article

A Non-canonical PDK1-RSK Signal Diminishes Pro-caspase-8-Mediated Necroptosis Blockade

Zhang-Hua Yang,[1,4] Xiao-Nan Wu,[3,4] Peng He,[1,4] Xuekun Wang,[1] Jianfeng Wu,[1] Tingting Ai,[1] Chuan-Qi Zhong,[1] Xiurong Wu,[1] Yu Cong,[1] Rongfeng Zhu,[1] Hongda Li,[1] Zhi-Yu Cai,[1] Wei Mo,[1,2,*] and Jiahuai Han[1,2,5,*]

[1]State Key Laboratory of Cellular Stress Biology, Innovation Center for Cell Biology, School of Life Sciences, Xiamen University, Xiamen, Fujian 361102, China

[2]Research Unit of Cellular Stress of CAMS, Cancer Research Center of Xiamen University, Xiang'an Hospital of Xiamen University, School of Medicine, Xiamen University, Xiamen, Fujian 361102, China

[3]School of Pharmaceutical Sciences, Xiamen University, Xiamen, Fujian 361102, China

[4]These authors contributed equally

[5]Lead Contact

*Correspondence: wmo@xmu.edu.cn (W.M.), jhan@xmu.edu.cn (J.H.)

https://doi.org/10.1016/j.molcel.2020.09.004

SUMMARY

Necroptosis induction *in vitro* often requires caspase-8 (Casp8) inhibition by zVAD because pro-Casp8 cleaves RIP1 to disintegrate the necrosome. It has been unclear how the Casp8 blockade of necroptosis is eliminated naturally. Here, we show that pro-Casp8 within the necrosome can be inactivated by phosphorylation at Thr265 ($pC8^{T265}$). $pC8^{T265}$ occurs *in vitro* in various necroptotic cells and in the cecum of TNF-treated mice. p90 RSK is the kinase of pro-Casp8. It is activated by a mechanism that does not need ERK but PDK1, which is recruited to the RIP1-RIP3-MLKL-containing necrosome. Phosphorylation of pro-Casp8 at Thr265 can substitute for zVAD to permit necroptosis *in vitro*. $pC8^{T265}$ mimic T265E knockin mice are embryonic lethal due to unconstrained necroptosis, and the pharmaceutical inhibition of RSK-mediated $pC8^{T265}$ diminishes TNF-induced cecum damage and lethality in mice by halting necroptosis. Thus, phosphorylation of pro-Casp8 at Thr265 by RSK is an intrinsic mechanism for passing the Casp8 checkpoint of necroptosis.

INTRODUCTION

Necroptosis can be induced by the activation of tumor necrosis factor receptor (TNFR) superfamily receptors, Toll-like receptor (TLR)3 and TLR4, interferon receptors (IFNRs) or pathogen infections (Han et al., 2011). All of these necroptosis-inducing signals converge on receptor-interacting protein kinase-3 (RIP3) (Cho et al., 2009; He et al., 2009; Zhang et al., 2009), which interacts with RIP1 or other RHIM-containing proteins through its RIP homology-interacting motif (RHIM) domain (Sun et al., 2002) to form a large amyloid-like signaling complex named necrosome (Li et al., 2012). Activated RIP3 within necrosome recruits and phosphorylates its downstream target mixed lineage kinase domain-like protein (MLKL) to trigger MLKL activation (Sun et al., 2012; Zhao et al., 2012). Activated MLKLs oligomerize and translocate to the plasma membrane to execute necroptosis (Cai et al., 2014; Chen et al., 2014; Dondelinger et al., 2014; Wang et al., 2014).

The necroptotic process is blocked by pro-caspase-8 (pro-Casp8) in the necrosome as forced inhibition of Casp8 by caspase inhibitor such as zVAD (benzyloxycarbonyl-valine-alanine-aspartic acid-fluoromethyl ketone) is a must-do step to induce necroptosis in many types of cells upon death stimulus (Degterev et al., 2005; Holler et al., 2000). The loss of Casp8 or Fas-associated protein with death domain (FADD), a linker between RIP1 and Casp8, leads to necroptosis in the mouse embryo, which supports the idea that pro-Casp8 blocks RIP3-mediated necroptosis *in vivo* (Dillon et al., 2012; Kaiser et al., 2011; Oberst et al., 2011; Zhang et al., 2011). The protease activity of pro-Casp8 is required for inhibiting necroptosis, while its self-cleaved product, mature Casp8, promotes apoptosis. Mechanically, pro-Casp8 may form heterodimers with $cFLIP_L$ (cellular FLICE-like inhibitory protein long, also known as CFLAR) to cleave necrosome components that promote necroptosis (Oberst et al., 2011). Several substrates of pro-Casp8 in the TNF signaling pathway have been identified, such as RIP1 (Lin et al., 1999), RIP3 (Feng et al., 2007), and deubiquitinase CYLD (O'Donnell et al., 2011), and studies have revealed that the cleavage of RIP1 by pro-Casp8 is the main mechanism to limit necroptosis *in vivo* (Lalaoui et al., 2020; Newton et al., 2019a; Tao et al., 2020).

The artificial addition of zVAD for necroptotic induction challenges the physiological relevance of those *in vitro* studies for a long time despite increasing evidence has demonstrated that necroptosis does occur *in vivo*, with important contributions to not only normal embryonic development but also the

Please cite this article in press as: Yang et al., A Non-canonical PDK1-RSK Signal Diminishes Pro-caspase-8-Mediated Necroptosis Blockade, Molecular Cell (2020), https://doi.org/10.1016/j.molcel.2020.09.004

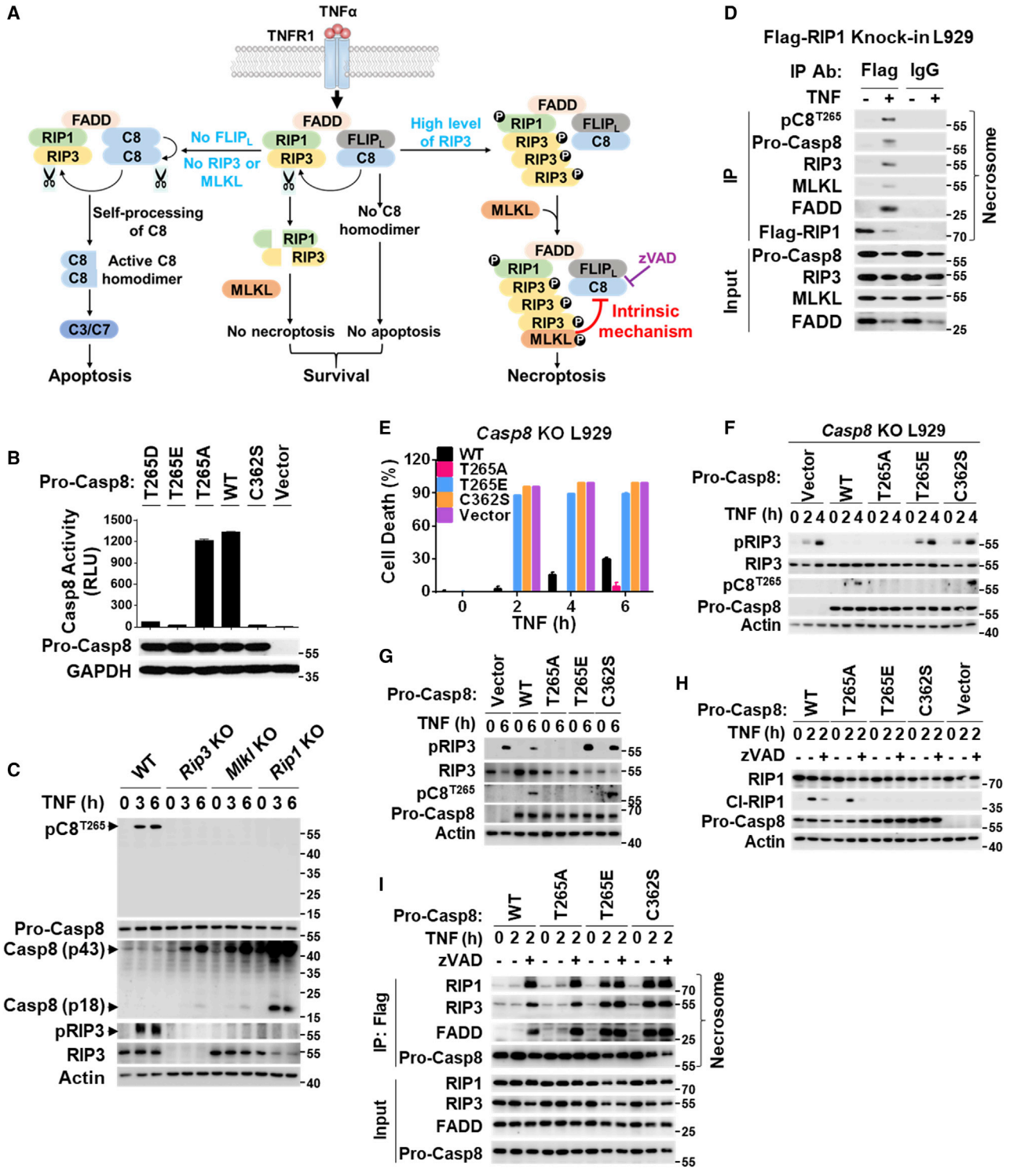

Figure 1. Phosphorylation of Pro-Casp8 at Thr265 Passes the Casp8 Checkpoint of Necroptosis in Cells

(A) Graphic model for the tight regulation of cell death pathway upon TNF stimulation. C8, caspase-8.

(B) HEK293T cells were transfected with a vector encoding nothing (vector), inactive form Casp8 (C362S), T265 phosphomimetic, or phosphodefective mutants of Casp8. Casp8 activities were analyzed 24 h after transfection. Pro-Casp8 protein levels were measured by immunoblotting with anti-FLAG antibody. Data are presented as means ± SDs of triplicates. RLU, relative luminescence unit.

(legend continued on next page)

pathogenesis of numerous diseases, including TNF-mediated systemic inflammatory response syndrome (SIRS), ischemia-reperfusion (IR) injury, neurodegeneration diseases, and infectious disorders (Jouan-Lanhouet et al., 2014). The needlessness of zVAD in TNF-triggered necroptosis *in vivo* and in a few cell lines such as L929 suggests that there must be an unknown intrinsic mechanism(s) to overcome the Casp8 blockade of necroptosis.

The activity of Casp8 could be regulated by protein modifications such as phosphorylation or ubiquitination (Zamaraev et al., 2017). However, none of them was shown to participate in necroptosis. In this study, we discovered that the phosphorylation of pro-Casp8 at Thr265 by p90 ribosomal S6 kinase (RSK) abolished Casp8 activity, leading to the preservation of necrosome integrity and subsequent necroptosis. The RSK family of kinases has four members (RSK1, RSK2, RSK3, and RSK4), which promote cell survival, growth, and proliferation (Anjum and Blenis, 2008). RSKs contain N- and C-terminal kinase domains. The C-terminal kinase of RSK is activated when Ser380 is phosphorylated by extracellular signal regulated kinase (ERK) which then permits Ser221 site phosphorylation by phosphoinositide-dependent protein kinase-1 (PDK1, also known as PDPK1) to activate N-terminal kinase (Houles and Roux, 2018). We found in this study that the activation of the N-terminal kinase of RSK in TNF-treated cells does not require C-terminal kinase activation by ERK, but is still mediated by PDK1. This non-canonical activation mechanism is followed by the recruitment of RSK to the necrosome, where it phosphorylates pro-Casp8 at Thr265. Like the artificial inhibition of pro-Casp8 by zVAD, Thr265 phosphorylation of pro-Casp8 stabilizes the necrosome and pushes the signaling balance toward necroptosis. The necroptosis-mediated embryonic lethality of the *Casp8*$^{T265E/T265E}$ mouse and the protective effects of the pharmaceutical inhibition of RSKs in TNF-treated mice support the idea that the inactivation of pro-Casp8 by RSK is an intrinsic mechanism that allows the passing of the Casp8 blockade of necroptosis *in vitro* and *in vivo* in certain organs/tissues.

RESULTS

There Is an Intrinsic Mechanism that Overcomes the Necroptosis Blockade by Pro-Casp8

Studies with HT29, Jurkat T, NIH 3T3, and mouse embryonic fibroblast (MEF) cells, as well as mouse models, revealed that pro-Casp8 safeguards cells against necroptosis (Cho et al., 2009; Günther et al., 2011; He et al., 2009; Kaiser et al., 2011; Oberst et al., 2011; Zhang et al., 2009). RIP1 and possibly RIP3 are constantly cleaved by pro-Casp8 complexed with cFLIP$_L$ (Green et al., 2011; Lu et al., 2011; Oberst et al., 2011), which disrupts the necrosome and stops the process of necroptosis (Figure 1A [graphic model]). Meanwhile, cFLIP$_L$ also inhibits apoptotic pro-Casp8 self-processing (Figure 1A). The pan-caspase inhibitor zVAD is commonly used in the induction of necroptosis *in vitro* by blocking pro-Casp8 activity, whereas murine fibroblast cell line L929 is among the few cell lines that undergo necroptosis in response to TNF stimulation with no need of additional pro-Casp8 inhibition (Vercammen et al., 1997), suggesting that pro-Casp8 in the necrosome can be disarmed by an intrinsic mechanism (Figure 1A). We note that the effect of the forced inhibition of pro-Casp8 by zVAD is more potent than that by the intrinsic mechanism, as zVAD can further enhance TNF-induced necroptosis in L929 cells (Vercammen et al., 1998). As expected, the deletion of *cFLIP$_L$* in L929 cells led to pro-Casp8 self-processing and apoptosis upon TNF stimulation, and zVAD preserved and further enhanced necroptosis in these cells, as indicated by the phosphorylation of RIP3 (pRIP3) and MLKL (pMLKL) (Figures S1A–S1C). Interestingly, the deletion of *Rip3* or *Mlkl* also led to pro-Casp8 self-processing-initiated apoptosis as that of *cFLIP$_L$* deletion in TNF-treated L929 cells, but no necroptosis can be initiated (Figures S1D–S1F). As MLKL recruitment is an event after RIP3 oligomerization and autophosphorylation (Sun et al., 2012; Wu et al., 2014), the presence of MLKL in the necrosome is required for the suppression of pro-Casp8 self-processing. This notion is supported by data that the reconstitution of *Rip3* knockout (KO) cells with kinase-dead or RHIM domain mutated RIP3, which cannot recruit MLKL, failed to suppress pro-Casp8 self-processing (Figures S1G–S1I). Thus, in addition to cFLIP$_L$, the presence of RIP3 and MLKL in the necrosome is required for the suppression of pro-Casp8 self-processing (Figure 1A). As the suppression of pro-Casp8 self-processing couples with the capability of pro-Casp8 to block necroptosis, the intrinsic mechanism that disarms the pro-Casp8 gatekeeper of necroptosis should only be activated after MLKL recruitment (Figure 1A).

Rip1 deletion leads to the pathway switch to a fast TRADD-dependent apoptosis (Vanlangenakker et al., 2011), which is not related to the topic of the present study and is not discussed here.

(C) T265 phosphorylation of pro-Casp8 was determined with anti-phospho-T265 Casp8 (pC8^{T265}) antibody in wild-type (WT), *Rip1* knockout (KO), *Rip3* KO, and *Mlkl* KO L929 cells treated with TNF (10 ng/mL) for different periods of time. Phosphorylation on T231 and S232 of RIP3 (pRIP3) was detected by anti-phospho-RIP3 antibody.

(D) Immunoprecipitation with anti-FLAG or anti-IgG antibody was performed in FLAG-RIP1 knockin L929 cells stimulated with TNF (10 ng/mL) for 2 h. The cell lysates and immunoprecipitates were analyzed by immunoblotting with antibodies as indicated.

(E) *Casp8* KO L929 cells reconstituted with pro-Casp8 or its mutants were treated with TNF (10 ng/mL) for different periods, as indicated. Cell death was measured. Data are presented as means ± SDs of triplicates.

(F) The same cells as in (E) were treated with TNF for periods, as indicated, and the cell lysates were analyzed by immunoblotting to detect the phosphoproteins and proteins as indicated.

(G) The same cells as in (E) were treated with TNF for 6 h, and the cell lysates were analyzed by immunoblotting as in (F).

(H) The same cells as in (E) were treated with TNF or TNF+zVAD (20 μM) for 2 h and the cell lysates were analyzed by immunoblotting to detect the proteins as indicated. Cl-RIP1, cleaved RIP1.

(I) Immunoprecipitation with anti-FLAG was performed in FLAG-Casp8 reconstituted L929 cells stimulated with TNF or TNF+zVAD for 2 h. The cell lysates and immunoprecipitates were analyzed by immunoblotting to detect the proteins as indicated.

See also Table S1 and Figures S1 and S2.

Please cite this article in press as: Yang et al., A Non-canonical PDK1-RSK Signal Diminishes Pro-caspase-8-Mediated Necroptosis Blockade, Molecular Cell (2020), https://doi.org/10.1016/j.molcel.2020.09.004

The Intrinsic Mechanism Leads to Phosphorylation of Pro-Casp8 at Thr265

To explore the mechanism of how the pro-Casp8-mediated blockade of necroptosis is suppressed, we examined a number of possibilities, including the phosphorylation of pro-Casp8. Mass spectrometric analysis revealed 9 potential phosphorylation sites in Casp8 (Table S1). We mutated each of these sites to phosphomimetic glutamic acid (E) and overexpressed these mutants in 293T cells. The enzymatically defective pro-Casp8 mutant C362S was included in the experiment as a control. T265E, but not other mutants, showed a similar reduction in Casp8 activity to that of C362S (Figure S1J). Both E and D (aspartic acid) but not A mutation of Thr265 eliminated pro-Casp8 activity (Figure 1B). Furthermore, by expressing the p18 fragment of Casp8 or its T265A, T265E, and C362S mutants into 293T cells together with p10 fragment of Casp8, we found that the phosphomimetic mutation of Thr265 also eliminated the activity of mature Casp8 (Figure S1K). Of note, the homodimerization of pro-Casp8 was not influenced by Thr265 phosphorylation (Figure S1L). Structure analysis of human CASP8 suggested that the phosphorylation of human CASP8 Thr263, which corresponds to mouse Casp8 Thr265, may affect the interactions with surrounding residues and induce local conformational changes that rearrange the substrate-binding pocket (Figures S1M–S1P).

To determine whether the phosphorylation of pro-Casp8 at Thr265 ($pC8^{T265}$) occurs in necroptosis, we generated a specific antibody to $pC8^{T265}$. The specificity of anti-$pC8^{T265}$ had been verified in *Casp8* KO L929 cells by western blot (Figure S2A) and immunofluorescence assay (Figure S2B), as well as in 293T cells overexpressed with phosphorylation site mutants and WT pro-Casp8 by western blot (Figure S2C). $pC8^{T265}$ was detected on pro-Casp8 after TNF treatment in L929 cells but vanished in *Rip3*, *Mlkl*, or *Rip1* KO cells (Figure 1C). $pC8^{T265}$ was also detected in the necroptosis of different types of cells, including MEFs (Figure S2D, TNF+zVAD; TNF+SM164+zVAD; TNF+CHX+zVAD), NIH 3T3-A cells expressing RIP3 (Figure S2E, TNF; TNF+zVAD), Raw264.7 (Figure S2F, TNF+zVAD; LPS+-zVAD), and L929 (Figure S2G, TNF; HSV-1+zVAD), but not in the apoptosis of those cells. Notably, $pC8^{T265}$ was clearly bound to the necrosome immunoprecipitated by FLAG-RIP1 from TNF-treated FLAG-RIP1 knockin L929 cells (Figure 1D), demonstrating that $pC8^{T265}$ was present in the necrosome. We further analyzed the presence of $pC8^{T265}$ *in vivo* in TNF-treated mice. It is known that cecum is the most sensitive organ to TNF-induced necroptosis (Chen et al., 2015). We observed $pC8^{T265}$ in epithelial cells of damaged cecum from wild-type (WT) mice, but not from $Rip3^{-/-}$ or $Rip3^{-/-}Casp8^{-/-}$ mice (Figure S2H). Collectively, we discovered pro-Casp8 phosphorylation at Thr265 in the necrosome, which abolished its enzymatic activity.

To determine whether pro-Casp8 with Thr265 phosphorylation can no longer halt necroptosis, *Casp8* KO L929 cells reconstituted with pro-Casp8 or its variant mutants were examined. More and quicker deaths occurred in cells reconstituted with vector, T265E, or C362S mutant than those with WT or T265A mutant (Figure 1E). Using pRIP3 as the marker of necroptosis, further analysis of the TNF-2h and -4h samples revealed the occurrence of necroptosis in *Casp8* KO cells with vector, T265E, or C362S mutant but not in those with WT or T265A (Figure 1F). These data demonstrated that the phosphomimetic T265E in pro-Casp8 disabled its ability to halt necroptosis (pRIP3). Consistent with the role of $pC8^{T265}$ in inactivating pro-Casp8, T265A-reconstituted cells cannot undergo necroptosis, as pRIP3 was still not detected at TNF-6h (Figure 1G). In line with the published results and data above, we were able to detect the cleavage of RIP1 in WT or T265A reconstituted cells in TNF-2h samples but not in T265E, C362S, or vector reconstituted cells (Figure 1H). The interplay between necrosome assembling and disintegrating was very well presented in WT reconstituted cells: the cleavage of RIP1 and the phosphorylation of Thr265 in pro-Casp8 at early time points (Figures 1H, 1F, and S2I) and the appearance of pRIP3 later (Figures 1G and S2I). Similar results were observed when cells were treated with herpes simplex virus 1 (HSV-1) (Figures S2J and S2K). Of note, adopting the phosphomimetic T265E mutant into the non-cleavable pro-Casp8 (DA-T265E) also disabled its ability to halt necroptosis (pRIP3) (Figure S2L), emphasizing that the phosphorylation of full-length Casp8 at Thr265 abolished its activity.

We analyzed necrosome formation in TNF-2h samples in detail (Figure 1I), in which the necrosome was not detected in WT and T265A reconstituted cells but appeared where zVAD had been pre-included in the culture medium. This is consistent with a widely accepted notion that pro-Casp8 disintegrated the necrosome, and the inhibition of pro-Casp8 by zVAD pushed the balance toward the stabilization of the necrosome (Green et al., 2011). As expected, zVAD was not required for necrosome formation in the cells reconstituted with T265E or the enzymatically inactive C362S mutant (Figure 1I), demonstrating that Thr265 phosphorylation of pro-Casp8 can substitute for zVAD in diminishing the blockade of necroptosis by pro-Casp8.

Thr265 Phosphomimetic Mutation in Pro-Casp8 Impairs the Blockade of Necroptosis during Embryo Development

To validate $pC8^{T265}$ function *in vivo*, we generated $Casp8^{T265E/T265E}$, $Casp8^{T265A/T265A}$, and $Casp8^{C362S/C362S}$ knockin mice, respectively (Figures S3A and S3B). The expression level of pro-Casp8 in T265E and T265A mice was similar to that in WT mice (Figure S3C), indicating that the phosphorylation of pro-Casp8 at Thr265 has no effect on its protein stability. $Casp8^{T265A/T265A}$ mice were viable and did not display any gross physical or behavioral abnormalities (Figure S3D). Cecum from $Casp8^{T265A/T265A}$ mice was used as a negative control for the immunostaining of $pC8^{T265}$ in TNF-treated mice (Figure S3E).

As with $Casp8^{C362S/C362S}$ mice (Fritsch et al., 2019), $Casp8^{T265E/T265E}$ mice were embryonic lethal (Figures 2A, 2B, S3F, and S3G), which is similar to what was observed with *Casp8* deletion (Kaiser et al., 2011; Oberst et al., 2011; Varfolomeev et al., 1998). No living embryos of $Casp8^{T265E/T265E}$ and $Casp8^{C362S/C362S}$ mice were found at embryonic day 12.5 (E12.5) (Figures 2A and S3G). Hyperemia in the abdominal region can be detected in some of the $Casp8^{T265E/T265E}$ or $Casp8^{C362S/C362S}$ embryos from E10.5 (Figures S3H and S3I), and the dead embryos had abnormal yolk sac vasculature (Figures 2B, 2C, and S3H–S3J). Immunostaining of pRIP3 revealed robust necroptosis in the yolk sac of $Casp8^{T265E/T265E}$ mice

Please cite this article in press as: Yang et al., A Non-canonical PDK1-RSK Signal Diminishes Pro-caspase-8-Mediated Necroptosis Blockade, Molecular Cell (2020), https://doi.org/10.1016/j.molcel.2020.09.004

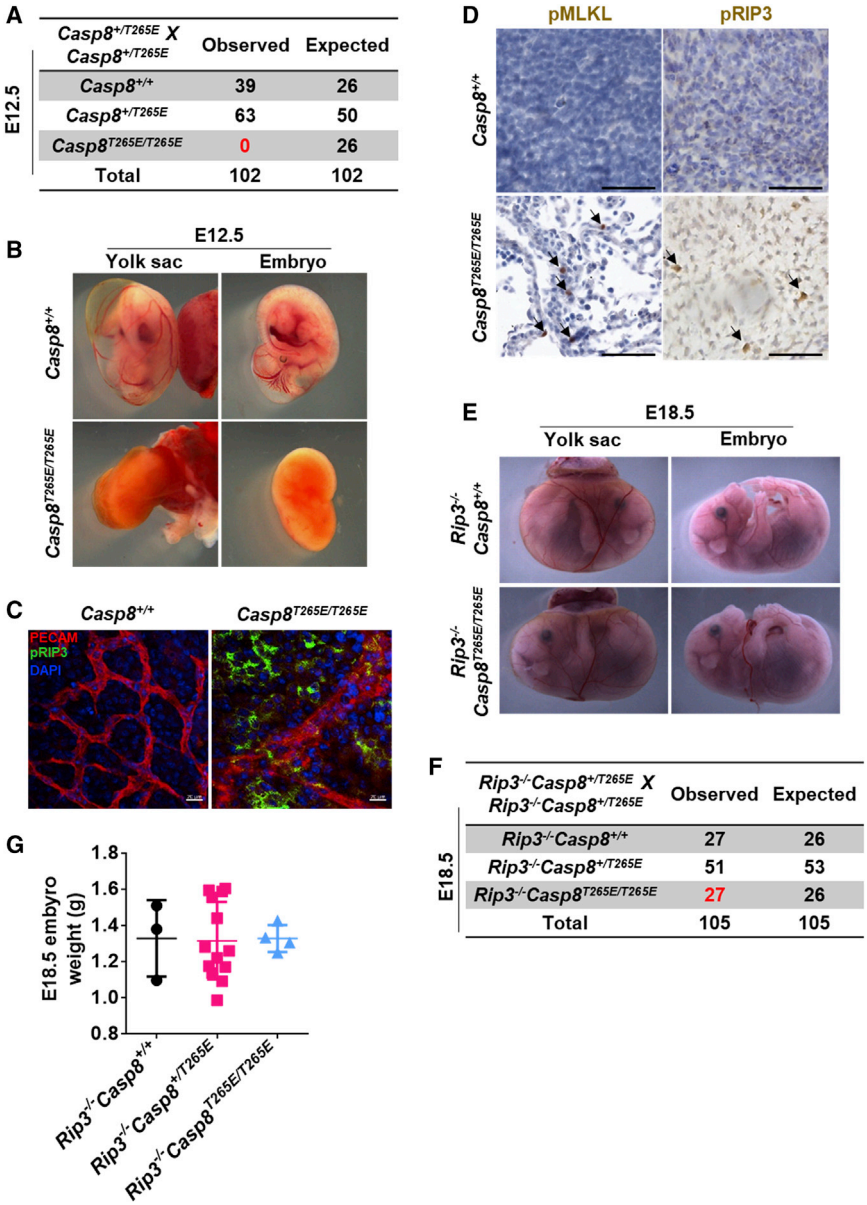

Figure 2. Phosphorylation of Pro-Casp8 at Thr265 Releases the Blockade of Necroptosis in Mice Embryos

(A) Expected and observed frequency of *Casp8*$^{+/T265E}$ offspring at E12.5 from intercross.

(B) Representative photographs of E12.5 embryos with the indicated genotype. The right panel shows sideby-side embryos with yolk sacs removed. Original magnification ×100.

(C) PECAM-1 (CD31) and phospho-RIP3 (pRIP3) staining of a whole-mount E12.5 yolk sac from the indicated genotype (×400). Scale bar, 20 μm.

(D) Embryo of WT (*Casp8*$^{+/+}$) or *Casp8*$^{T265E/T265E}$ mouse at E11.5 was sectioned and stained with phospho-RIP3 (pRIP3) and phospho-MLKL (pMLKL). Scale bar, 20 μm.

(E) Representative photographs of E18.5 embryos with the indicated genotype. The right panel shows side-by-side embryos with yolk sacs removed. Original magnification ×75.

(F) Expected and observed frequency of *Rip3*$^{-/-}$ *Casp8*$^{+/T265E}$ offspring at E18.5 from intercross.

(G) Body weight of E18.5 embryos of indicated genotypes.

See also Figures S3 and S4.

(Figure 2C). Immunohistochemistry (IHC) staining of pRIP3 and pMLKL presented overflowing necroptosis in the embryo of *Casp8*$^{T265E/T265E}$ mice (Figure 2D), indicating that pC8^{T265} allowed necroptosis to occur *in vivo*. Consistently, the embryonic lethality between E10.5 and E12.5 of *Casp8*$^{T265E/T265E}$ mice could be fully rescued by deleting either *Rip3* or *Mlkl* (Figures 2E, 2F, S3K, and S3L). At E18.5, the weight of *Rip3*$^{-/-}$*Casp8*$^{T265E/T265E}$ or *Mlkl*$^{-/-}$ *Casp8*$^{T265E/T265E}$ embryos was similar to their *Casp8*$^{+/+}$ littermates (Figures 2G and S3K). Of note, in contrast to *Rip3*$^{-/-}$ *Casp8*$^{-/-}$ and *Mlkl*$^{-/-}$*Casp8*$^{-/-}$ mice that are viable, all *Mlkl*$^{-/-}$ *Casp8*$^{T265E/T265E}$ mice died during the perinatal period (Figure S3M), and ~10% (6 of 64) *Rip3*$^{-/-}$*Casp8*$^{T265E/T265E}$ mice survived beyond weaning (Figure S3N). The viability of *Mlkl*$^{-/-}$ *Casp8*$^{T265E/T265E}$ and *Rip3*$^{-/-}$*Casp8*$^{T265E/T265E}$ mice/embryos was similar to the recently reported *Rip3*$^{-/-}$*Casp8*^{C362SC362S} and *Mlkl*$^{-/-}$*Casp8*$^{C362S/C362S}$ (Fritsch et al., 2019), *Rip3*$^{-/-}$*Casp8*$^{C362A/C362A}$, and *Mlkl*$^{-/-}$*Casp8*$^{C362A/C362A}$ mice/embryos (Newton et al., 2019b). We also observed obvious villus atrophy in the *Rip3*$^{-/-}$*Casp8*$^{T265E/T265E}$ and *Mlkl*$^{-/-}$ *Casp8*$^{T265E/T265E}$ embryos at E18.5 (Figure S4A). *Rip3*$^{-/-}$*Casp8*$^{T265E/T265E}$ mice showed markedly stunted growth (Figures S4B and S4C) and suffered from anemia, splenomegaly, and mild immune cell infiltrations in tissues such as the liver (Figures S4D–S4G). The splenomegaly may result from the expansion of the red pulp by extramedullary hematopoiesis (Figure S4G). We then compared Casp8 (T265E) with Casp8 (C362S) and Casp8 (C362A) in cells. The pro-Casp8 (C362S) or (C362A) appears to act as a scaffold to nucleate ASC speck assembly for the activation of the inflammasome, which then causes lethality in mice (Fritsch et al., 2019, Newton et al., 2019b), and we also detected ASC specks in the intestines of a *Mlkl*$^{-/-}$ *Casp8*$^{T265E/T265E}$ embryo at E18.5 (Figure S4H). Casp8 (C362S) and Casp8 (C362A) had a propensity to enter the Triton X-100 insoluble cellular fraction as did Casp8 (T265E), which led to co-expressed ASC entering of the Triton X-100 insoluble cellular fraction (Figure S4I). These data demonstrated that the T265E mutation in Casp8 greatly resembled the function of C362S or C362A mutation in mice and cells.

RSKs Phosphorylate Pro-Casp8 at Thr265

As the phosphorylation of Thr265 occurred in the necrosome, we tested RIP1, RIP3, and MLKL and found that none of these

Please cite this article in press as: Yang et al., A Non-canonical PDK1-RSK Signal Diminishes Pro-caspase-8-Mediated Necroptosis Blockade, Molecular Cell (2020), https://doi.org/10.1016/j.molcel.2020.09.004

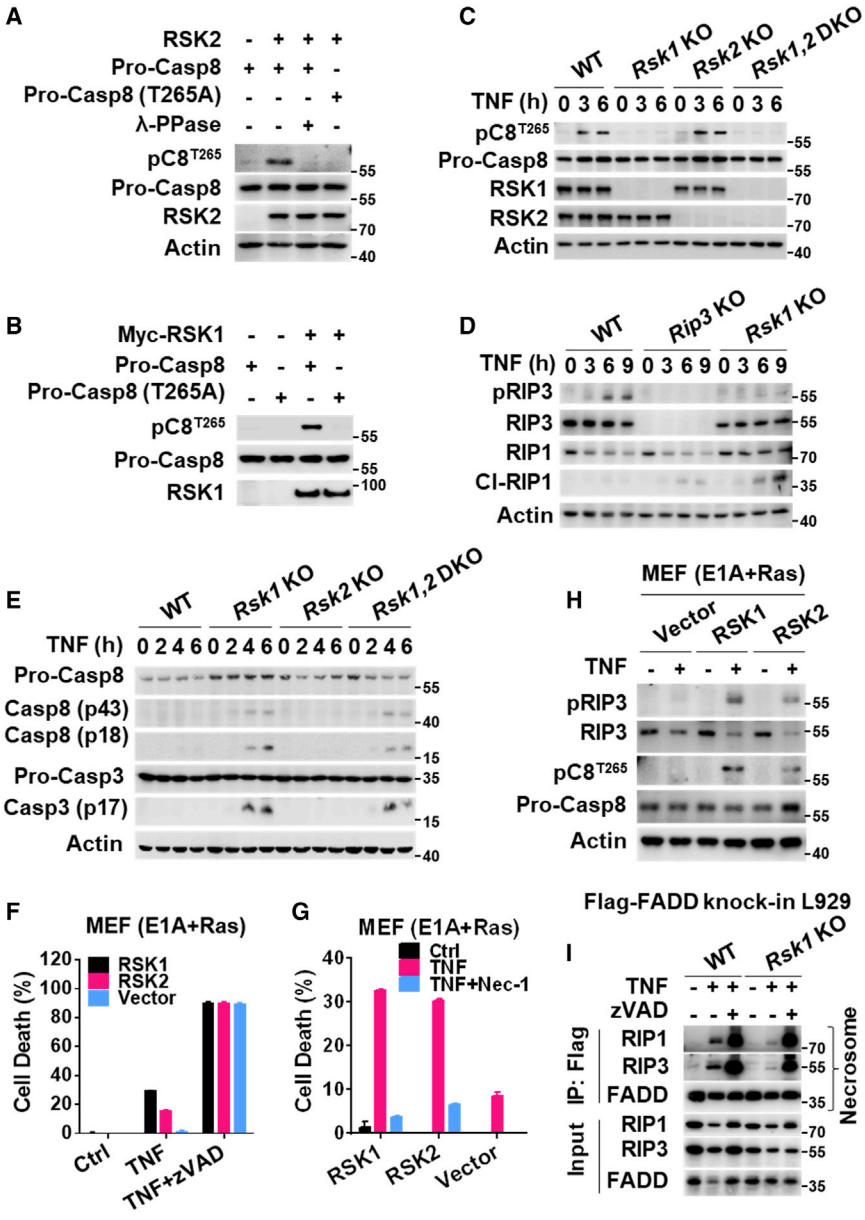

Figure 3. RSKs Mediate Phosphorylation of Pro-Casp8 at Thr265

(A) RSK2 was co-expressed with FLAG-pro-Casp8 or FLAG-pro-Casp8 (T265A) in 293T cells. FLAG-pro-Casp8 was immunoprecipitated using anti-FLAG antibody and then incubated with or without λ-phosphatase (λ-PPase) for 30 min at 25°C. The pro-Casp8 and pC8^{T265} in immunoprecipitates were analyzed with anti-pC8^{T265} and anti-FLAG antibodies. Cell lysates were immunoblotted with anti-RSK2 and anti-actin antibodies.

(B) RSK1 and pro-Casp8 were co-transfected in 293T, and the cell lysates were analyzed by immunoblotting 24 h post-transfection.

(C) T265 phosphorylation of pro-Casp8 in WT, *Rsk1* KO, *Rsk2* KO, and *Rsk1, Rsk2* DKO L929 cells treated with TNF (10 ng/mL) for different periods.

(D) WT, *Rip3* KO, and *Rsk1* KO L929 cells were treated with TNF, and the cell lysates were analyzed by immunoblotting to detect the phosphoproteins and proteins as indicated.

(E) WT, *Rsk1* KO, *Rsk2* KO, and *Rsk1*, *Rsk2* DKO L929 cells were treated with TNF for different periods as indicated, and the cleavage of Casp8 and Casp3 was analyzed by immunoblotting.

(F) E1A+Ras-transformed MEF cells overexpressing RSK1 or RSK2 were treated with TNF (100 ng/mL) or TNF+zVAD (20 μM). Cell death was measured. Data are presented as means ± SDs of triplicates.

(G) The same cells as in (F) were treated with TNF or TNF+Nec-1 (30 μM). Cell death was measured. Data are presented as means ± SDs of triplicates.

(H) The same cells as in (F) were treated with TNF, and the cell lysates were analyzed as indicated.

(I) Immunoprecipitation with anti-FLAG antibody was performed in 3xFLAG-FADD knockin, *Rsk1* WT, or KO L929 cells stimulated with TNF (8 h) or TNF+zVAD (2 h). The cell lysates and immunoprecipitates were analyzed by immunoblotting to detect the proteins as indicated.

See also Figure S5.

necrosome components can phosphorylate Casp8 (data not shown). A database and literature search revealed that Thr263 in human CASP8 (the corresponding site of Thr265 in mouse Casp8) can be phosphorylated by RSK2 (Peng et al., 2011). The RSK family of kinases consists of four members (RSK1, RSK2, RSK3, and RSK4) that share a high degree of sequence homology (Houles and Roux, 2018). We tested RSK2 and RSK1 using *in vitro* kinase assays and found that both can directly phosphorylate mouse pro-Casp8 at Thr265 (Figures 3A and 3B). To determine whether RSKs are the pro-Casp8 kinase in necroptosis, we genetically deleted *Rsk1*, *Rsk2*, or both in L929 cells and examined TNF-induced pC8^{T265} (Figure 3C). Deletion of *Rsk1* but not *Rsk2* eliminated TNF-induced pC8^{T265} (Figure 3C). The selective function of RSK1 is most likely due to that RSK1 is the predominantly expressed RSK in L929 cells (Figure S5A). This notion is supported by the data that the knockdown of *Rsk2*, the major RSK expressed in NIH 3T3 cells (Figure S5B), attenuated TNF-induced pro-Casp8 suppression and pRIP3 in this cell line (Figures S5C and S5D). The deletion of *Rsk1* in L929 cells facilitated the disintegration of the necrosome as indicated by the cleavage of RIP1 (Figure 3D) and apoptotic activation of Casp8 and Casp3 (Figures 3E and S5E). Overall, *Rsk1* deletion phenocopies *Rip3* or *Mlkl* KO in L929 cells (Figures S1D, S1E, S5F, and S5G).

To demonstrate that the RSK-mediated phosphorylation of pro-Casp8 is an intrinsic mechanism that can substitute for zVAD in promoting necroptosis in cultured cells, we used an E1A+Ras transformed MEF cell line that underwent necroptosis in response to the treatment of TNF+zVAD but not TNF alone (Newton et al., 2014) and overexpressed RSK1 or RSK2 in this cell line (Figure S5H). The overexpression of either RSK1 or RSK2 sensitized the cells to TNF-alone-induced death

(Figure 3F), and the necroptotic nature of cell death was indicated by inhibition with the RIP1 inhibitor Nec-1 (Figure 3G) and the occurrence of pRIP3 and pC8^{T265} (Figure 3H). We note that the effect of RSK overexpression on necroptosis is not as strong as that of zVAD treatment. This is reasonable, as the phosphorylation of pro-Casp8 by RSK takes multiple steps such as RSK recruitment and molecular interactions between RSK and Casp8, and the overexpression of RSK-mediated pro-Casp8 phosphorylation may be much less than 100%. TNF alone is able to induce necroptosis in L929 cells, and the deletion of *Rsk1* in L929 cells reduced necrosome (Figure 3I). Meanwhile, zVAD was still able to promote necrosome formation in *Rsk1* KO L929 cells (Figure 3I), confirming the substitutable nature between zVAD and RSK in preventing pro-Casp8 from stopping the necroptotic process.

RSK Is Recruited to MLKL-Containing Necrosome

Next, we sought to determine where RSK phosphorylates pro-Casp8. Since the necrosome in TNF+zVAD-treated cells is much easier to detect than that in TNF-treated cells, the immunoprecipitations of RSK1 were performed using the cells treated with or without TNF+zVAD. We detected pro-Casp8, FADD, RIP1, RIP3, and MLKL in the immunoprecipitation of RSK1 from WT L929 cells but not in *Rip3* KO cells (Figure 4A). We also showed that RSK1 can be specifically pulled down by RIP3 from TNF+zVAD-treated L929 cells and TNF+SM164+-zVAD-treated MEF cells (Figures 4B and 4C). These data indicated that RSK is associated with the necrosome after TNF stimulation. Interestingly, deleting *Mlkl* deprived RSK1 from the RIP3 immunoprecipitates, but it did not affect the presence of RIP1, FADD, and pro-Casp8 (Figure 4D), and the absence of RSK1 had no effect on the formation of RIP1, RIP3, FADD, pro-Casp8, and MLKL complex (Figure 4E). Thus, the recruitment of RSK1 to the necrosome occurs after MLKL being a part of the necrosome. The recruitment of RSK1 does not require pro-Casp8, FADD, and RIP1 since RSK1 can be recruited to the RIP3-MLKL complex induced by artificial RIP3 dimerization (Figure 4F) (Wu et al., 2014).

RSK Is Activated by an ERK-Independent but PDK1-Dependent Mechanism in TNF-Treated Cells

RSK family members have two kinase domains, N-terminal kinase domain (NTKD) and C-terminal kinase domain (CTKD) (Anjum and Blenis, 2008). The well-established activation mechanism of a given RSK is that ERK phosphorylates and activates its CTKD, which in turn auto-phosphorylates Ser380 (mouse RSK1 amino acid numbering) in a hydrophobic motif. PDK1 can be recruited to the phosphorylated hydrophobic motif to phosphorylate S221 (mouse RSK1 amino acid numbering) and activate the NTKD (Anjum and Blenis, 2008; Houles and Roux, 2018). NTKD phosphorylates all known RSK substrates (Figure S6A [graphic model]). We could detect TNF-induced S380 and S221 phosphorylation of RSK1 (pRSK [S221] and pRSK [S380]) in L929 cells, as well as ERK1/2 phosphorylation (pERK) under serum-free conditions, but not in the presence of serum (Figures 5A and S6B), which should be due to that serum-mediated basal RSK activation masked TNF-induced RSK1 activation. Similarly, we detected strong basal RSK activation (pRSK [S221] signal) in the epithelial cells of the cecum by immunostaining and were unable to detect changes in the level of pRSK (S221) or RSK1 protein after TNF treatment (data not shown). Although serum (growth factors)-mediated RSK activation is predominant, TNF-induced RSK activation appeared to be unique since blocking TNF-induced ERK1/2 activation (phosphorylation) by the MEK inhibitor PD98059 eliminated the increase in pS380 but not pS221 in RSK1 (Figure 5A), while in contrast, PD98059 effectively eliminated epidermal growth factor (EGF)-induced pS380 and pS221 in L929 cells (Figure S6C). PD98059 also had no effect on pC8^{T265} and pRIP3 (Figure 5A), indicating that the phosphorylation of S380 is not required for pC8^{T265}. These data suggest that although the canonical activation mechanism exists in TNF-treated L929 cells, the majority of TNF-induced pS221 of RSK1 is executed by a mechanism that is different from that shown in the graphic model of Figure S6A.

ERK-mediated RSK activation is CTKD dependent (Dalby et al., 1998; Smith et al., 1999) (Figure S6A [graphic model]). However, NTKD activity was detected in overexpressed CTKD kinase-dead mutants or CTKD-deletion mutants of RSK (Bjørbaek et al., 1995; Fisher and Blenis, 1996), which suggests the presence of CTKD-independent RSK1 activation. We reconstituted RSK1 expression in RSK1 knockdown L929 cells with RSK1 WT or mutant of CTKD kinase-dead, NTKD kinase-dead, CTKD+NTKD kinase-dead, NTKD alone, and CTKD alone. TNF-induced pC8^{T265} and pRIP3 were detected in the cells as long as NTKD was restored, even with NTKD reconstitution alone (Figures 5B and S6E). The induction of pC8^{T265} correlated well with Casp8 activity (Figures 5C and S6D). We also found that the NTKD portion but not the CTKD portion of RSK1 was recruited to the necrosome (Figure S6F). BI-D1870 and SL0101 are kinase inhibitors of NTKD and FMK is for CTKD (Houles and Roux, 2018). BI-D1870 and SL0101 but not FMK attenuated pC8^{T265}, which allowed the increase of Casp8 activity and halted necroptosis in TNF-treated L929 cells (Figures 5D–5F). TNF-induced Casp8 activity in *Rsk1* and *2* double KO (DKO) and *Rip3* KO cells was not influenced by BI-D1870, confirming that RSK was specifically targeted by this compound during necroptosis (Figure S6G). A similar effect of BI-D1870 was observed by using NIH 3T3-A+RIP3 cells (Figures S6H and S6I). Collectively, TNF-induced RSK1 activation for pC8^{T265} is via a mechanism independent of the CTKD of RSK1.

PDK1 is the known kinase that activates the NTKD of RSK (Jensen et al., 1999) (Figure S6A [graphic model]).Importantly, PDK1 inhibitor GSK470 effectively inhibited S221 phosphorylation in TNF-treated L929 cells to a level below background, but it had no effect on S380 phosphorylation (Figure S6J). The p38 pathway was also reported to mediate S380 phosphorylation of RSK (Zaru et al., 2007), and we found that p38 inhibitors SB203580 and BIRB796, as well as JNK inhibitor SP600125, had no effect on TNF-induced pS380 and pS221 (Figure S6J). A similar result was obtained in MEF cells (Figure S6K). Similar to RSK inhibition by BI-D1870, the inhibition of PDK1 also significantly attenuated pC8^{T265}, which allowed Casp8 activation and halted necroptosis in TNF-treated L929 cells (Figures 5G–5I). Moreover, the genetic deletion of *Pdk1* in L929 cells dramatically

Please cite this article in press as: Yang et al., A Non-canonical PDK1-RSK Signal Diminishes Pro-caspase-8-Mediated Necroptosis Blockade, Molecular Cell (2020), https://doi.org/10.1016/j.molcel.2020.09.004

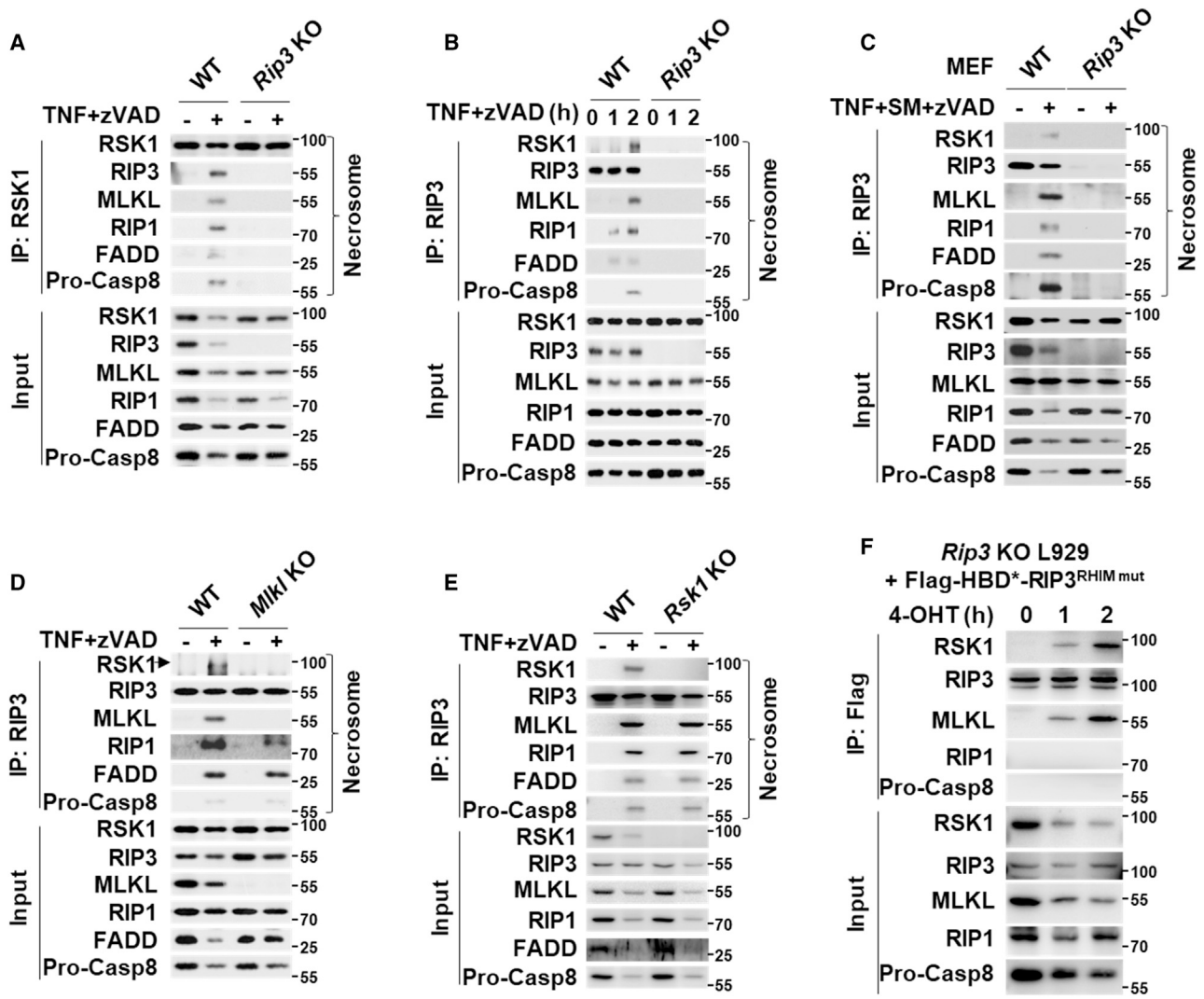

Figure 4. RSK1 Takes Part in Necrosome after MLKL Has Been Recruited

(A) Immunoprecipitation with anti-RSK1 antibody was performed in WT and *Rip3* KO L929 cells stimulated with TNF+zVAD (20 μM) for 2 h. The cell lysates and immunoprecipitates were analyzed by immunoblotting to detect the proteins as indicated.

(B) Immunoprecipitation with anti-RIP3 antibody was performed in WT and *Rip3* KO L929 cells stimulated with TNF+zVAD for 2 h. The cell lysates and immunoprecipitates were analyzed as in (A).

(C) MEF cells were treated with or without TNF+SM164+zVAD for 2 h. The cell lysates were immunoprecipitated with anti-RIP3 antibody and analyzed as in (A).

(D and E) Immunoprecipitation with anti-RIP3 antibody was performed in WT and *Mlkl* KO L929 cells (D) or in *Rsk1* KO L929 cells (E) stimulated with TNF+zVAD for 2 h. The cell lysates and immunoprecipitates were analyzed as in (A).

(F) *Rip3* KO L929 cells reconstituted with FLAG-HBD*-RIP3 (RHIM mut) were treated with 4-OHT (1 μM). The cell lysates were immunoprecipitated with FLAG antibody and analyzed as indicated.

decreased TNF-induced pC8^{T265} and pRIP3, resulting in the increase in Casp8 activity and the decrease in necroptosis (Figures 5J–5L). Importantly, the re-expression of PDK1 in *Pdk1*-deficient L929 cells restored TNF-induced necroptosis and inhibited Casp8 activation (Figures 5M, 5N, and S6L). Thus, the ERK-independent activation of RSK by PDK1 inactivates pro-Casp8 and promotes necroptosis.

PDK1 is broadly expressed and constitutively active (Alessi et al., 1997). The current model of S221 phosphorylation by PDK1 requires the docking of PDK1 to the S380 phosphorylated hydrophobic motif in RSK (Frödin et al., 2000) (Figure S6A). However, in TNF-treated L929 cells, S380A RSK1 functions as WT RSK1 in restoring TNF-induced pS221 of RSK1, pC8^{T265}, and pRIP3 (Figure 5O), but S221A RSK1 mutant cannot support RSK1-mediated pC8^{T265} and pRIP3 (Figure 5O). Likewise, the induction of necroptosis and the suppression of Casp8 activation were impaired in cells expressing S221A mutant RSK1 (Figures S6M and S6N). These data showed that the canonical ERK-PDK1 axis-mediated RSK activation and the pS380-independent RSK activation by PDK1 are

Please cite this article in press as: Yang et al., A Non-canonical PDK1-RSK Signal Diminishes Pro-caspase-8-Mediated Necroptosis Blockade, Molecular Cell (2020), https://doi.org/10.1016/j.molcel.2020.09.004

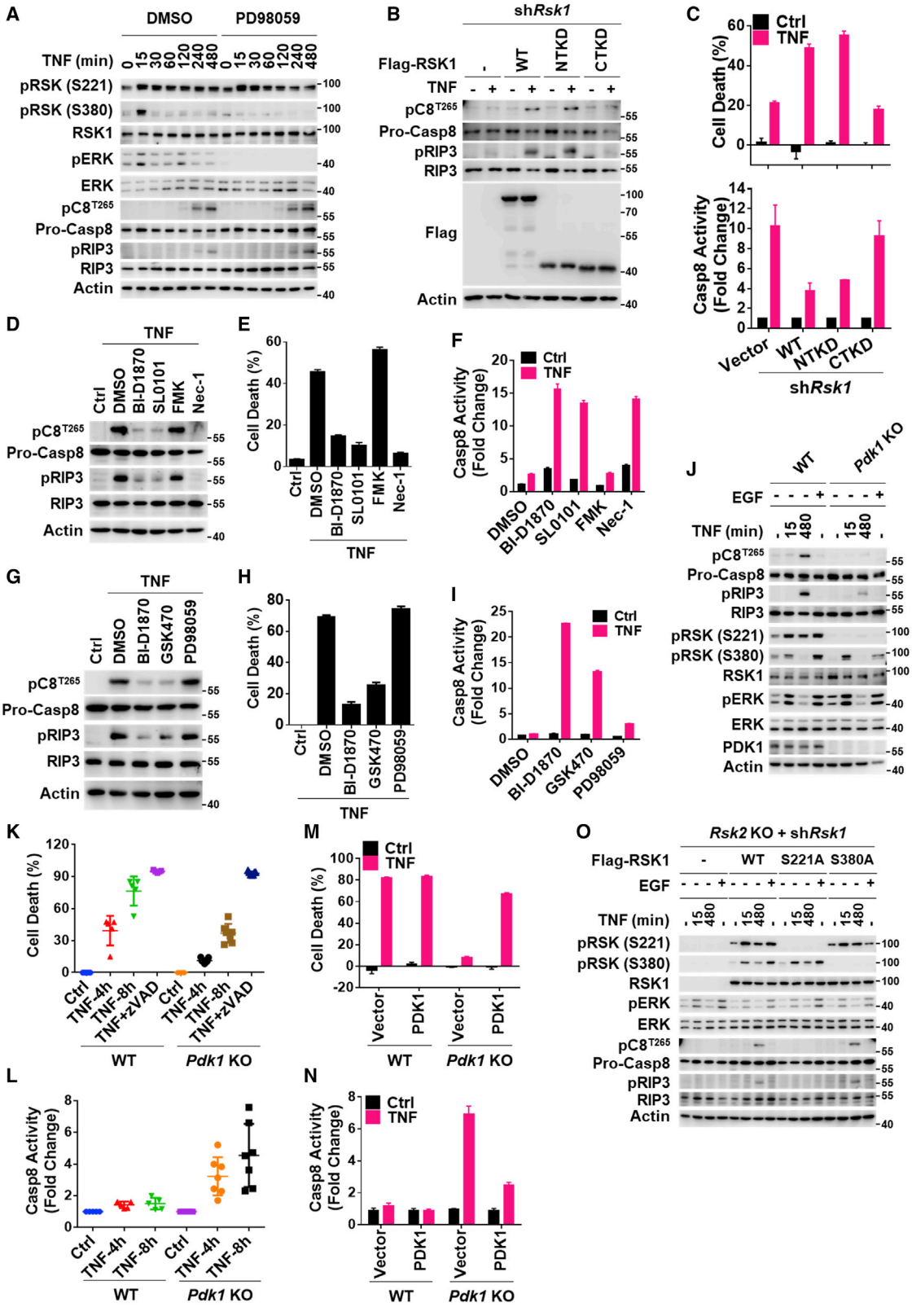

(legend on next page)

Please cite this article in press as: Yang et al., A Non-canonical PDK1-RSK Signal Diminishes Pro-caspase-8-Mediated Necroptosis Blockade, Molecular Cell (2020), https://doi.org/10.1016/j.molcel.2020.09.004

distinct mechanisms. The latter does not require the ERK and CTKD of RSK. Collectively, the RSK activation by TNF in L929 cells is mediated by PDK1 in a previously unknown mechanism independent of ERK.

The RSK family of kinases can be activated by ERKs in a vast majority of cases. Peng et al. (2011) reported first that RSK2 phosphorylated human CASP8 at Thr263 and negatively regulated the function of CASP8 downstream of TNFR family member Fas. Their study suggested that EGF induces human CASP8 phosphorylation, which promotes pro-CASP8 degradation. However, we were unable to detect EGF-induced pC8^{T265} (Figure S6O) and protein instabilization (Figures S6P and S6Q). We also did not detect changes in the protein stability of pro-Casp8 in TNF-treated L929 cells (Figure S6R). We could conclude that promoting protein degradation is not the mechanism to inhibit Casp8 during necroptosis, but this mechanism may function in other cellular processes.

Pharmaceutical Inhibition of RSKs Protects Mice from TNF-Induced Cecum Injury and Lethality

Given the fact that inhibitors of NTKD of RSK attenuate TNF-induced necroptosis *in vitro*, we further tested it *in vivo*. WT mice were injected intravenously with 300 μg/kg recombinant murine TNF, and all of the mice succumbed within 24 h (Figure 6A). BI-D1870 protected 80% mice from TNF-induced lethality during the first 24 h, and 60% of the mice were fully recovered thereafter (Figure 6A). Conversely, BI-D1870 failed to protect *Casp8*$^{T265A/T265A}$ mice from TNF-induced death, excluding the possibility that the off-target effects of BI-D1870 protected mice from TNF-induced death (Figure 6B). The cecum has been described as an organ whose injury is mainly mediated by TNF-induced necroptosis (Chen et al., 2015). We further analyzed the effect of RSK inhibitor on TNF-induced cecum injury and found that in the BI-D1870 treatment group, cecum damage was significantly compromised (Figures 6C and 6D). The number of pC8^{T265+} cells was dramatically decreased, as was the number of necroptotic cells (pMLKLs) (Figures 6E and 6F). Thus, RSK plays a key role in TNF-induced necroptosis in cecum and lethality in WT mice.

The Phosphorylation-Mediated Inactivation of Casp8 Functions *In Vivo* in an Organ/Tissue-Restricted Manner

The functions of phosphomimetic (T265E) and phosphodefect (T265A) mutants of Casp8 in cell lines and embryo development (Figures 1, 2, S2, and S3) support the role of phosphorylation-mediated inactivation of Casp8 in necroptosis. The data of MEFs that were isolated from E9.5 embryos of WT, *Casp8*$^{C362S/C362S}$, *Casp8*$^{T265E/T265E}$, and *Casp8*$^{T265A/T265A}$ and transformed with E1A&Ras, which allowed the transformed MEFs to undergo necroptosis upon TNF plus zVAD treatment (Newton et al., 2014), also support the role of the inactivation of Casp8 by phosphorylation in promoting necroptosis (Figure 7A). Although the cells or embryos containing the T265A mutant of Casp8 behaved similarly to those containing WT Casp8, one would expect the necroptotic effect of TNF in *Casp8*$^{T265A/T265A}$ mice to be weaker than that observed in WT mice, as RSK-mediated inactivation of Casp8 cannot take place on T265A Casp8. We used a series of TNF doses to treat WT and *Casp8*$^{T265A/T265A}$ mice and found that the lethal effect of TNF in *Casp8*$^{T265A/T265A}$ mice was unexpectedly stronger than that in WT mice (Figure 7B). Tissues were collected when a mouse became moribund, and apparent hemorrhagic lesions were observed in the cecum of WT mice but not in that of *Casp8*$^{T265A/T265A}$ mice (Figure 7C). Consistently, the signals of pMLKL were significantly reduced in the cecum of *Casp8*$^{T265A/T265A}$ mice (Figure 7D). These data indicated that TNF-induced necroptosis and damage in the cecum were compromised in *Casp8*$^{T265A/T265A}$ mice, confirming the role of phosphorylation-mediated inhibition of Casp8 in necroptosis *in vivo*. Strikingly, gross hemorrhage was found in the small intestine of *Casp8*$^{T265A/T265A}$ but not in WT mice (Figure 7C). Histological analysis demonstrated marked destruction of the architecture and obvious signs of hemorrhage in the small intestine but not in the colon or cecum of *Casp8*$^{T265A/T265A}$ mice challenged with TNF (Figure 7E). Furthermore, the small intestine of *Casp8*$^{T265A/T265A}$ mice contained a large increase in the numbers of cleaved-Casp3^{+} cells as well as pMLKL^{+} cells (Figures 7F and 7G). Damage to the small intestine should be the cause of mortality of TNF-treated *Casp8*$^{T265A/T265A}$ mice because it was the only organ damage found in low dose (100 μg/kg)

Figure 5. RSK Is Activated by an ERK-Independent but PDK1-Dependent Mechanism in TNF-Treated Cells

(A) L929 cells deprived of serum for 24 h were pre-treated with DMSO or PD98059 (20 μM) for 1 h, followed by TNF treatment as indicated. The cell lysates were analyzed by immunoblotting.

(B and C) *Rsk1* knockdown L929 cells were reconstituted with vector, RSK1, or truncates (CTKD, C-terminal kinase domain; NTKD, N-terminal kinase domain). After 6 h of TNF stimulation, the cell lysates were analyzed by immunoblotting (B). The cell death and Casp8 activities (C) were measured. Data are presented as means ± SDs of triplicates.

(D–F) L929 cells were pre-treated with RSK inhibitors (BI-D1870: 10 μM; SL0101: 100 μM; FMK: 10 μM) or RIP1 inhibitor Nec-1 (30 μM) for 1 h and then treated with TNF (10 ng/mL) for 6 h. The cell lysates were analyzed by immunoblotting to detect the proteins as indicated (D). Cell death (E) and the Casp8 activities were measured (F). Data are presented as means ± SDs of triplicates.

(G–I) L929 cells were pre-treated with inhibitors (PD98059: 20 μM; BI-D1870: 10 μM; GSK470: 10 μM) for 2 h and then treated with TNF for 6 h. The cell lysates were analyzed by immunoblotting (G). The cell death (H) and Casp8 activities (I) were measured. Data are presented as means ± SDs of triplicates.

(J) WT and *Pdk1* KO L929 cells deprived of serum for 24 h were treated with EGF (100 ng/mL, 5 min) or TNF (10 ng/mL), as indicated, and the cell lysates were analyzed by immunoblotting.

(K and L) Cell death (K) and Casp8 activity (L) in WT (n = 5 clones) and *Pdk1* KO (n = 7 clones) L929 cells treated as indicated. Data are presented as means ± SDs.

(M and N) WT and *Pdk1* KO L929 cells were re-expressed with HA-PDK1 and treated with TNF for 6 h. The cell death (M) and Casp8 activities (N) were measured. Data are presented as means ± SDs of triplicates.

(O) *Rsk1* knockdown *Rsk2* KO L929 cells were reconstituted with vector, WT RSK1 or RSK1 mutants. The cells deprived of serum for 24 h were treated with EGF (100 ng/mL, 5 min) or TNF (10 ng/mL) as indicated, and the cell lysates were analyzed by immunoblotting.

See also Figure S6.

Please cite this article in press as: Yang et al., A Non-canonical PDK1-RSK Signal Diminishes Pro-caspase-8-Mediated Necroptosis Blockade, Molecular Cell (2020), https://doi.org/10.1016/j.molcel.2020.09.004

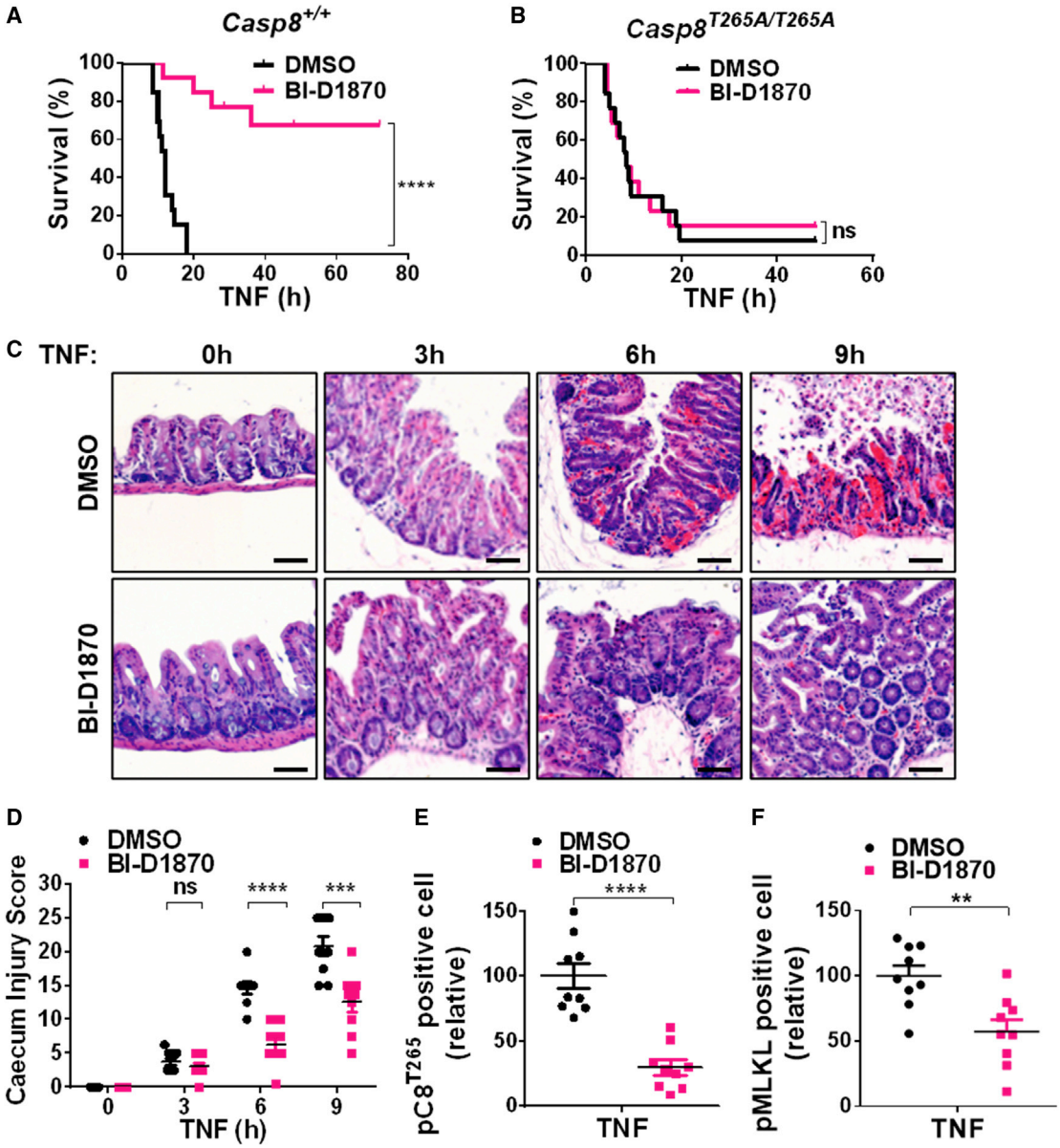

Figure 6. Pharmaceutical Inhibition of RSKs Protects Mice from TNF-Induced Cecum Injury and Lethality

(A and B) C57BL/6 wild-type (*Casp8*$^{+/+}$) mice or *Casp8*$^{T265A/T265A}$ mice were intravenously (i.v.) injected with 10 mg/kg BI-D1870 or vehicle at 1 h before 300 μg/kg TNF i.v. injection. Mouse survival was presented as a Kaplan-Meier plot, and the log-rank test was performed. n = 13 for each group pooled from 3 independent experiments.

(C and D) C57BL/6 mice were i.v. injected with 10 mg/kg BI-D1870 or vehicle and then i.v. injected with 300 μg/kg TNF 1 h later. Cecum was collected at the indicated time points, sectioned, and stained with H&E. The representative images are shown in (C). At the 0 h time point, n = 4 mice for each group. At other time points, n = 10 mice. Scale bar, 50 μm. The TNF-induced cecum damage at the indicated time point was scored (see Method Details) and is shown in (D).

(E and F) The same cecum as in (C) was stained with pMLKL antibody or pC8^{T265} antibody. The relative amounts of pC8^{T265+} cells (E) or pMLKL^{+} cells (F) were counted and shown. ns, $p \geq 0.05$; *$p < 0.05$; **$p < 0.01$; ***$p < 0.001$; ****$p < 0.0001$. All of the results are representative of 2 or 3 independent experiments.

TNF-challenged *Casp8*$^{T265A/T265A}$ mice, and small intestine damage correlated with the death of *Casp8*$^{T265A/T265A}$ mice (Figure 7H). Collectively, the phosphorylation-mediated inactivation of Casp8 functions in the cecum, but the effect of the Casp8 (T265A) mutant in the small intestine is not related to the cecum-restricted antinecroptotic effect of this mutation, and most likely to an additional, yet unknown, function of Casp8, which may have no relation to the T265 phosphorylation of Casp8.

DISCUSSION

Because pro-Casp8 in the necrosome constitutively cleaves RIP1, the necrosome should be in dynamic assembling and

Please cite this article in press as: Yang et al., A Non-canonical PDK1-RSK Signal Diminishes Pro-caspase-8-Mediated Necroptosis Blockade, Molecular Cell (2020), https://doi.org/10.1016/j.molcel.2020.09.004

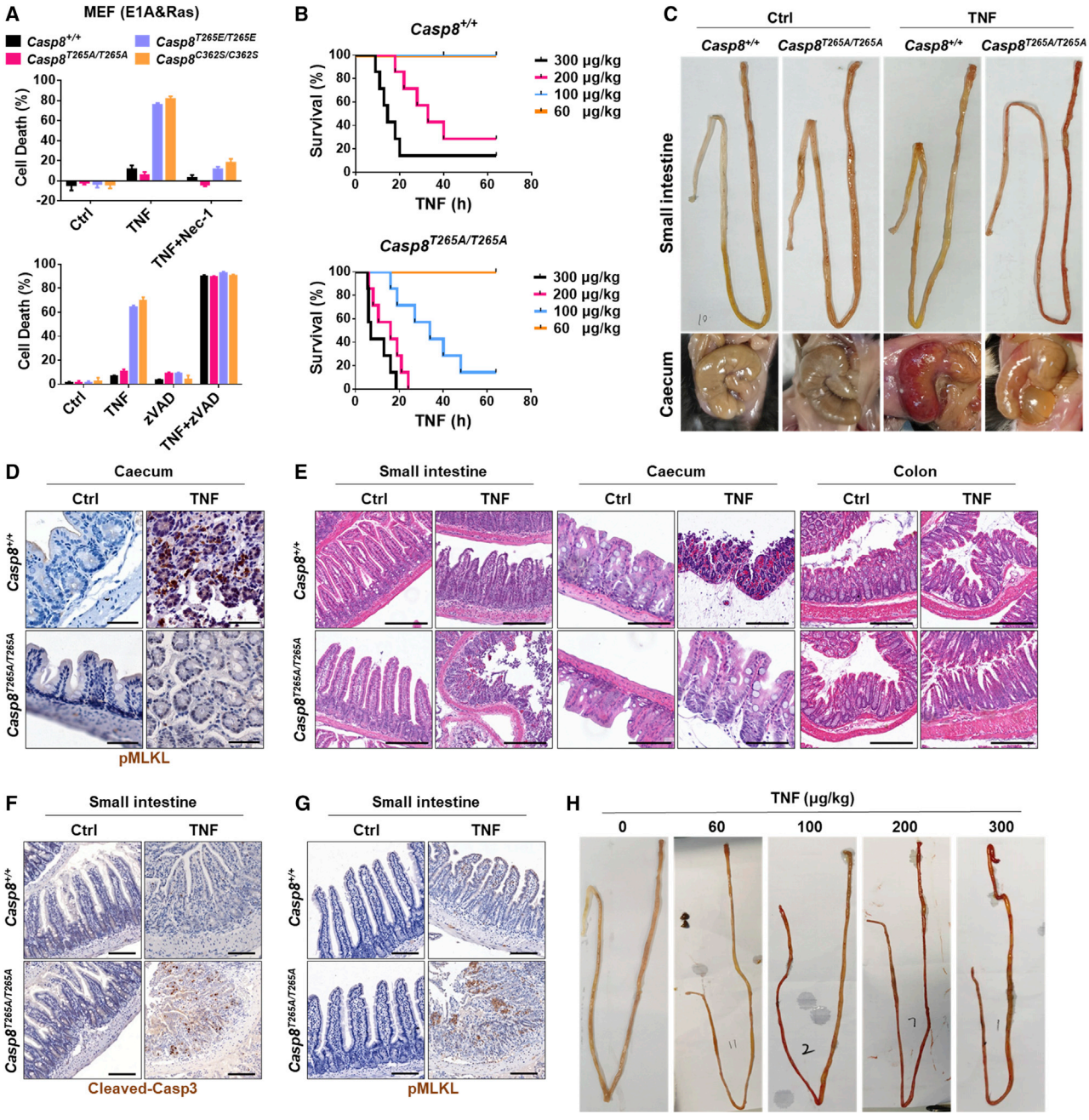

Figure 7. The Phosphorylation-Mediated Inactivation of Casp8 Functions *In Vivo* in an Organ/Tissue-Restricted Manner

(A) E1A+Ras-transformed MEF cells of indicated genotypes were treated with TNF (100 ng/mL), TNF+Nec-1 (30 μM), or TNF+zVAD (20 μM). Cell death was measured. Data are presented as means ± SDs of triplicates.

(B) *Casp8*$^{+/+}$ or *Casp8*$^{T265A/T265A}$ mice were i.v. injected with a series of doses of TNF. Mouse survival was presented as a Kaplan-Meier plot, and the log-rank test was performed. n = 7 for each group.

(C) Representative images of gastrointestinal tract from moribund *Casp8*$^{+/+}$ or *Casp8*$^{T265A/T265A}$ mice i.v. injected with 300 μg/kg TNF.

(D) Cecum from (C) was stained with pMLKL antibody. Scale bar, 50 μm.

(E) Tissues were collected when a mouse became moribund, sectioned, and stained with H&E. Representative images are shown. Scale bar, 200 μm.

(F and G) The small intestine from (E) was stained with cleaved-Casp3 antibody (F) or pMLKL antibody (G). Scale bar, 100 μm.

(H) Representative images of gastrointestinal tract from *Casp8*$^{T265A/T265A}$ mice i.v. injected with a series of doses of TNF. Tissues were collected when a mouse became moribund.

Please cite this article in press as: Yang et al., A Non-canonical PDK1-RSK Signal Diminishes Pro-caspase-8-Mediated Necroptosis Blockade, Molecular Cell (2020), https://doi.org/10.1016/j.molcel.2020.09.004

disintegrating in cells treated with necroptosis stimulus. We propose that this is a transient state of the necrosome. We show here in this study that RSK can be activated in TNF-treated cells by an ERK-independent but PDK1-dependent mechanism. RSK is then recruited to the necrosome, which stabilizes the transient necrosome by depriving pro-Casp8 activity and halting the disintegration of the necrosome, similar to what zVAD does in TNF-induced necroptosis. The accumulation of stable necrosomes finally triggers necroptotic cell death.

Pro-Casp8 in the necrosome may function as a gatekeeper to prevent unwanted necroptosis that leads to systematic inflammation. Previous work by Peng et al. (2011) has shown that in Jurkat T cells, the phosphorylation mutant of human CASP8, CASP8-T263A (Thr263 in human CASP8 is the corresponding site of Thr265 in mouse Casp8), is more active than WT in inducing apoptosis downstream of FAS. They found that the knockdown of RSK2 accelerated pro-Casp8 and pro-Casp3 processing and the accumulation of their cleavage products, and Casp8 and Casp3 activities were enhanced by suppressing RSK2 activity. Here, phosphorylation of pro-Casp8 by RSK in the necrosome is identified as an intrinsic mechanism for passing the Casp8 checkpoint of necroptosis. Several post-translational modifications of Casp8 have been reported (Zamaraev et al., 2017). Src family tyrosine kinases Src, Fyn, and Lyn can phosphorylate Casp8 at tyrosine 380 (Y380), which was implicated in apoptosis inhibition, cell migration, motility, and adhesion, as well as subcellular Casp8 localization. However, the phosphorylated Casp8 at tyrosine 380 (Y380) was not detected in necroptotic human cells. The phosphorylation of Casp8 by Cdk1-cyclin B1 or ERK1/2 at serine 387 (S390 in mouse) or by p38 at serine 347 had no effect on TNF-induced necroptosis (Figures 5 and S1J; data not shown). The ubiquitination of Casp8 is also not likely to be involved in necroptosis. The HECT domain containing E3 ubiquitin protein ligase 3 (HECTD3) mediates the K63 ubiquitination of Casp8 at K215, which apparently blocks the subsequent activation of Casp8 at the DISC through an undefined mechanism. TRAF2 also facilitated K48-linked ubiquitination of p18 Casp8 at the K224, K229, and K231 triad, which leads to the proteasomal degradation of auto-processed Casp8. Since passing the Casp8 checkpoint of necroptosis is controlled at pro-Casp8, the ubiquitination is not likely to be involved in the regulation of necroptosis.

RSKs are unique, with two distinct functional kinase domains. This study revealed that the N-terminal kinase activity of RSK is required to phosphorylate pro-Casp8 in the necrosome. However, the well-characterized activation mechanism (e.g., the sequential activation of the C-terminal kinase and the N-terminal kinase of RSK) does not play a role in the inactivation of pro-Casp8. The C-terminal kinase of RSK and the activation of the C-terminal kinase by ERK is not involved in TNF-induced activation of the N-terminal kinase of RSK (Figure 5A). Jensen et al. (1999) showed that the recombinant protein of the RSK2 N-terminal kinase domain had catalytic entity and its kinase activity increased when the Ser227 site was phosphorylated by PDK1. In the serum-starved cells, we observed the induction of phosphorylation at Ser221 of RSK1 by TNF stimulation under the condition that neither ERK activation nor phosphorylation of Ser380 at the linker region of RSK1 occurred (Figure 5). Thus, RSK1 in necroptotic cells is activated by PDK1 through a non-canonical mechanism.

The biological effect of RSK-mediated inactivation of Casp8 in embryo development and TNF-induced organ damage was demonstrated by using T265E and T265A knockin mice and a specific RSK inhibitor (Figures 2, 6, S3, and S4). While all of the data support the conclusion that inactivating Casp8 by RSK promotes necroptosis *in vivo*, the T265A knockin mouse also showed an unexpected phenotype upon TNF challenge (Figure 7). The small intestine in *Casp8*$^{T265A/T265A}$ mice became hypersensitive to TNF-induced injury. Cell death in the small intestine is a mix of apoptosis, necroptosis, and perhaps also other types of cell death. This phenomenon cannot be interpreted simply as a result of the possible increase in Casp8 enzymatic activity by T265A mutation, as the gain of unknown functions by T265A mutation also cannot be excluded. Treatment with RSK inhibitor BI-D1870 did not make a significant difference in small intestines from TNF-challenged mice (data not shown). Due to that the inhibition by the inhibitor cannot be complete, BI-D1870 cannot prove or disprove whether RSK-mediated inactivation is involved in the sensitivity of the small intestine to TNF-induced injury. Why it is cecum that is very sensitive to TNF-induced necroptosis in WT mice, why T265A mutation can only sensitize the small intestine but not other organs, and how the organ specificity or restriction applies to the cell death pathways are clearly important issues to be addressed in the future.

Perhaps due to the inflammatory nature of necroptosis (Pasparakis and Vandenabeele, 2015), the process of which is tightly controlled, the Casp8 checkpoint should be one of the self-guard mechanisms against inflammation. Understanding the intrinsic mechanism(s) that checks and releases the necroptotic process should provide clinical benefit to necroptosis-associated human diseases.

STAR★METHODS

Detailed methods are provided in the online version of this paper and include the following:

- KEY RESOURCES TABLE
- RESOURCE AVAILABILITY
  - Lead Contact
  - Materials Availability
  - Data and Code Availability
- EXPERIMENTAL MODEL AND SUBJECT DETAILS
  - Cell Culture
  - Mice
- METHOD DETAILS
  - SIRS Mouse Model
  - Histology
  - Immunofluorescence Microscopy
  - Generation of Knockout Cell Lines
  - Lentivirus Production and Infection
  - Immunoblotting and Immunoprecipitation
  - Mass Spectrometry Analysis
  - Cell Death Assay
  - Caspase-8 Activity Assay

SUPPLEMENTAL INFORMATION

Supplemental Information can be found online at https://doi.org/10.1016/j.molcel.2020.09.004.

ACKNOWLEDGMENTS

This work was supported by the National Natural Science Foundation of China (81788101 and 81630042 to J.H. and 31701204 to Z.-H.Y.), the National Scientific and Technological Major Project (2017ZX10202203-003 to J.H.), the 111 Project (B12001 to J.H.), research unit fund from the Chinese Academy of Medical Sciences (2019RU054 to J.H.), and the China Postdoctoral Science Foundation (2017M610396 and 2018T110648 to Z.-H.Y.).

AUTHOR CONTRIBUTIONS

Z.-H.Y., X.-N.W., and P.H. carried out the majority of the experimental work with help from X. Wu and X. Wang. J.W., T.A., and Y.C. provided relevant mice, and T.A. performed the H&E staining. C.-Q.Z. carried out the mass spectrometric analysis. H.L. and Z.-Y.C. performed pC8^{T265} IHC of the cecum. R.Z. performed the structural analysis. W.M. contributed comments and advice on the study and assisted with writing the manuscript. Z.-H.Y., X.-N.W., P.H., and J.H. designed the experiments and interpreted the data. Z.-H.Y., W.M., and J.H. wrote the manuscript. J.H. conceived and supervised the study.

DECLARATION OF INTERESTS

The authors declare no competing interests.

Received: April 27, 2020
Revised: August 17, 2020
Accepted: September 3, 2020
Published: September 25, 2020

REFERENCES

Alessi, D.R., Deak, M., Casamayor, A., Caudwell, F.B., Morrice, N., Norman, D.G., Gaffney, P., Reese, C.B., MacDougall, C.N., Harbison, D., et al. (1997). 3-Phosphoinositide-dependent protein kinase-1 (PDK1): structural and functional homology with the Drosophila DSTPK61 kinase. Curr. Biol. *7*, 776–789.

Anjum, R., and Blenis, J. (2008). The RSK family of kinases: emerging roles in cellular signalling. Nat. Rev. Mol. Cell Biol. *9*, 747–758.

Bjørbaek, C., Zhao, Y., and Moller, D.E. (1995). Divergent functional roles for p90rsk kinase domains. J. Biol. Chem. *270*, 18848–18852.

Cai, Z., Jitkaew, S., Zhao, J., Chiang, H.C., Choksi, S., Liu, J., Ward, Y., Wu, L.G., and Liu, Z.G. (2014). Plasma membrane translocation of trimerized MLKL protein is required for TNF-induced necroptosis. Nat. Cell Biol. *16*, 55–65.

Chen, W., Zhou, Z., Li, L., Zhong, C.Q., Zheng, X., Wu, X., Zhang, Y., Ma, H., Huang, D., Li, W., et al. (2013). Diverse sequence determinants control human and mouse receptor interacting protein 3 (RIP3) and mixed lineage kinase domain-like (MLKL) interaction in necroptotic signaling. J. Biol. Chem. *288*, 16247–16261.

Chen, X., Li, W., Ren, J., Huang, D., He, W.T., Song, Y., Yang, C., Li, W., Zheng, X., Chen, P., and Han, J. (2014). Translocation of mixed lineage kinase domain-like protein to plasma membrane leads to necrotic cell death. Cell Res. *24*, 105–121.

Chen, W., Wu, J., Li, L., Zhang, Z., Ren, J., Liang, Y., Chen, F., Yang, C., Zhou, Z., Su, S.S., et al. (2015). Ppm1b negatively regulates necroptosis through dephosphorylating Rip3. Nat. Cell Biol. *17*, 434–444.

Cho, Y.S., Challa, S., Moquin, D., Genga, R., Ray, T.D., Guildford, M., and Chan, F.K. (2009). Phosphorylation-driven assembly of the RIP1-RIP3 complex regulates programmed necrosis and virus-induced inflammation. Cell *137*, 1112–1123.

Coburn, B., Li, Y., Owen, D., Vallance, B.A., and Finlay, B.B. (2005). Salmonella enterica serovar Typhimurium pathogenicity island 2 is necessary for complete virulence in a mouse model of infectious enterocolitis. Infect. Immun. *73*, 3219–3227.

Dalby, K.N., Morrice, N., Caudwell, F.B., Avruch, J., and Cohen, P. (1998). Identification of regulatory phosphorylation sites in mitogen-activated protein kinase (MAPK)-activated protein kinase-1a/p90rsk that are inducible by MAPK. J. Biol. Chem. *273*, 1496–1505.

Degterev, A., Huang, Z., Boyce, M., Li, Y., Jagtap, P., Mizushima, N., Cuny, G.D., Mitchison, T.J., Moskowitz, M.A., and Yuan, J. (2005). Chemical inhibitor of nonapoptotic cell death with therapeutic potential for ischemic brain injury. Nat. Chem. Biol. *1*, 112–119.

Dillon, C.P., Oberst, A., Weinlich, R., Janke, L.J., Kang, T.B., Ben-Moshe, T., Mak, T.W., Wallach, D., and Green, D.R. (2012). Survival function of the FADD-CASPASE-8-cFLIP(L) complex. Cell Rep. *1*, 401–407.

Dondelinger, Y., Declercq, W., Montessuit, S., Roelandt, R., Goncalves, A., Bruggeman, I., Hulpiau, P., Weber, K., Sehon, C.A., Marquis, R.W., et al. (2014). MLKL compromises plasma membrane integrity by binding to phosphatidylinositol phosphates. Cell Rep. *7*, 971–981.

Feng, S., Yang, Y., Mei, Y., Ma, L., Zhu, D.E., Hoti, N., Castanares, M., and Wu, M. (2007). Cleavage of RIP3 inactivates its caspase-independent apoptosis pathway by removal of kinase domain. Cell. Signal. *19*, 2056–2067.

Fisher, T.L., and Blenis, J. (1996). Evidence for two catalytically active kinase domains in pp90rsk. Mol. Cell. Biol. *16*, 1212–1219.

Fritsch, M., Günther, S.D., Schwarzer, R., Albert, M.C., Schorn, F., Werthenbach, J.P., Schiffmann, L.M., Stair, N., Stocks, H., Seeger, J.M., et al. (2019). Caspase-8 is the molecular switch for apoptosis, necroptosis and pyroptosis. Nature *575*, 683–687.

Frödin, M., Jensen, C.J., Merienne, K., and Gammeltoft, S. (2000). A phosphoserine-regulated docking site in the protein kinase RSK2 that recruits and activates PDK1. EMBO J. *19*, 2924–2934.

Green, D.R., Oberst, A., Dillon, C.P., Weinlich, R., and Salvesen, G.S. (2011). RIPK-dependent necrosis and its regulation by caspases: a mystery in five acts. Mol. Cell *44*, 9–16.

Günther, C., Martini, E., Wittkopf, N., Amann, K., Weigmann, B., Neumann, H., Waldner, M.J., Hedrick, S.M., Tenzer, S., Neurath, M.F., and Becker, C. (2011). Caspase-8 regulates TNF-α-induced epithelial necroptosis and terminal ileitis. Nature *477*, 335–339.

Han, J., Zhong, C.Q., and Zhang, D.W. (2011). Programmed necrosis: backup to and competitor with apoptosis in the immune system. Nat. Immunol. *12*, 1143–1149.

He, S., Wang, L., Miao, L., Wang, T., Du, F., Zhao, L., and Wang, X. (2009). Receptor interacting protein kinase-3 determines cellular necrotic response to TNF-alpha. Cell *137*, 1100–1111.

Holler, N., Zaru, R., Micheau, O., Thome, M., Attinger, A., Valitutti, S., Bodmer, J.L., Schneider, P., Seed, B., and Tschopp, J. (2000). Fas triggers an alternative, caspase-8-independent cell death pathway using the kinase RIP as effector molecule. Nat. Immunol. *1*, 489–495.

Houles, T., and Roux, P.P. (2018). Defining the role of the RSK isoforms in cancer. Semin. Cancer Biol. *48*, 53–61.

Jensen, C.J., Buch, M.B., Krag, T.O., Hemmings, B.A., Gammeltoft, S., and Frödin, M. (1999). 90-kDa ribosomal S6 kinase is phosphorylated and activated by 3-phosphoinositide-dependent protein kinase-1. J. Biol. Chem. *274*, 27168–27176.

Jouan-Lanhouet, S., Riquet, F., Duprez, L., Vanden Berghe, T., Takahashi, N., and Vandenabeele, P. (2014). Necroptosis, in vivo detection in experimental disease models. Semin. Cell Dev. Biol. *35*, 2–13.

Kaiser, W.J., Upton, J.W., Long, A.B., Livingston-Rosanoff, D., Daley-Bauer, L.P., Hakem, R., Caspary, T., and Mocarski, E.S. (2011). RIP3 mediates the embryonic lethality of caspase-8-deficient mice. Nature *471*, 368–372.

Lalaoui, N., Boyden, S.E., Oda, H., Wood, G.M., Stone, D.L., Chau, D., Liu, L., Stoffels, M., Kratina, T., Lawlor, K.E., et al. (2020). Mutations that prevent caspase cleavage of RIPK1 cause autoinflammatory disease. Nature *577*, 103–108.

Li, J., McQuade, T., Siemer, A.B., Napetschnig, J., Moriwaki, K., Hsiao, Y.S., Damko, E., Moquin, D., Walz, T., McDermott, A., et al. (2012). The RIP1/RIP3 necrosome forms a functional amyloid signaling complex required for programmed necrosis. Cell *150*, 339–350.

Lin, Y., Devin, A., Rodriguez, Y., and Liu, Z.G. (1999). Cleavage of the death domain kinase RIP by caspase-8 prompts TNF-induced apoptosis. Genes Dev. *13*, 2514–2526.

Lu, J.V., Weist, B.M., van Raam, B.J., Marro, B.S., Nguyen, L.V., Srinivas, P., Bell, B.D., Luhrs, K.A., Lane, T.E., Salvesen, G.S., and Walsh, C.M. (2011). Complementary roles of Fas-associated death domain (FADD) and receptor interacting protein kinase-3 (RIPK3) in T-cell homeostasis and antiviral immunity. Proc. Natl. Acad. Sci. USA *108*, 15312–15317.

Newton, K., Dugger, D.L., Wickliffe, K.E., Kapoor, N., de Almagro, M.C., Vucic, D., Komuves, L., Ferrando, R.E., French, D.M., Webster, J., et al. (2014). Activity of protein kinase RIPK3 determines whether cells die by necroptosis or apoptosis. Science *343*, 1357–1360.

Newton, K., Wickliffe, K.E., Dugger, D.L., Maltzman, A., Roose-Girma, M., Dohse, M., Kőműves, L., Webster, J.D., and Dixit, V.M. (2019a). Cleavage of RIPK1 by caspase-8 is crucial for limiting apoptosis and necroptosis. Nature *574*, 428–431.

Newton, K., Wickliffe, K.E., Maltzman, A., Dugger, D.L., Reja, R., Zhang, Y., Roose-Girma, M., Modrusan, Z., Sagolla, M.S., Webster, J.D., and Dixit, V.M. (2019b). Activity of caspase-8 determines plasticity between cell death pathways. Nature *575*, 679–682.

O'Donnell, M.A., Perez-Jimenez, E., Oberst, A., Ng, A., Massoumi, R., Xavier, R., Green, D.R., and Ting, A.T. (2011). Caspase 8 inhibits programmed necrosis by processing CYLD. Nat. Cell Biol. *13*, 1437–1442.

Oberst, A., Dillon, C.P., Weinlich, R., McCormick, L.L., Fitzgerald, P., Pop, C., Hakem, R., Salvesen, G.S., and Green, D.R. (2011). Catalytic activity of the caspase-8-FLIP(L) complex inhibits RIPK3-dependent necrosis. Nature *471*, 363–367.

Pasparakis, M., and Vandenabeele, P. (2015). Necroptosis and its role in inflammation. Nature *517*, 311–320.

Peng, C., Cho, Y.Y., Zhu, F., Zhang, J., Wen, W., Xu, Y., Yao, K., Ma, W.Y., Bode, A.M., and Dong, Z. (2011). Phosphorylation of caspase-8 (Thr-263) by ribosomal S6 kinase 2 (RSK2) mediates caspase-8 ubiquitination and stability. J. Biol. Chem. *286*, 6946–6954.

Smith, J.A., Poteet-Smith, C.E., Malarkey, K., and Sturgill, T.W. (1999). Identification of an extracellular signal-regulated kinase (ERK) docking site in ribosomal S6 kinase, a sequence critical for activation by ERK in vivo. J. Biol. Chem. *274*, 2893–2898.

Sun, X., Yin, J., Starovasnik, M.A., Fairbrother, W.J., and Dixit, V.M. (2002). Identification of a novel homotypic interaction motif required for the phosphorylation of receptor-interacting protein (RIP) by RIP3. J. Biol. Chem. *277*, 9505–9511.

Sun, L., Wang, H., Wang, Z., He, S., Chen, S., Liao, D., Wang, L., Yan, J., Liu, W., Lei, X., and Wang, X. (2012). Mixed lineage kinase domain-like protein mediates necrosis signaling downstream of RIP3 kinase. Cell *148*, 213–227.

Tao, P., Sun, J., Wu, Z., Wang, S., Wang, J., Li, W., Pan, H., Bai, R., Zhang, J., Wang, Y., et al. (2020). A dominant autoinflammatory disease caused by non-cleavable variants of RIPK1. Nature *577*, 109–114.

Vanlangenakker, N., Bertrand, M.J., Bogaert, P., Vandenabeele, P., and Vanden Berghe, T. (2011). TNF-induced necroptosis in L929 cells is tightly regulated by multiple TNFR1 complex I and II members. Cell Death Dis. *2*, e230.

Varfolomeev, E.E., Schuchmann, M., Luria, V., Chiannilkulchai, N., Beckmann, J.S., Mett, I.L., Rebrikov, D., Brodianski, V.M., Kemper, O.C., Kollet, O., et al. (1998). Targeted disruption of the mouse Caspase 8 gene ablates cell death induction by the TNF receptors, Fas/Apo1, and DR3 and is lethal prenatally. Immunity *9*, 267–276.

Vercammen, D., Vandenabeele, P., Beyaert, R., Declercq, W., and Fiers, W. (1997). Tumour necrosis factor-induced necrosis versus anti-Fas-induced apoptosis in L929 cells. Cytokine *9*, 801–808.

Vercammen, D., Beyaert, R., Denecker, G., Goossens, V., Van Loo, G., Declercq, W., Grooten, J., Fiers, W., and Vandenabeele, P. (1998). Inhibition of caspases increases the sensitivity of L929 cells to necrosis mediated by tumor necrosis factor. J. Exp. Med. *187*, 1477–1485.

Wang, H., Sun, L., Su, L., Rizo, J., Liu, L., Wang, L.F., Wang, F.S., and Wang, X. (2014). Mixed lineage kinase domain-like protein MLKL causes necrotic membrane disruption upon phosphorylation by RIP3. Mol. Cell *54*, 133–146.

Wu, J., Huang, Z., Ren, J., Zhang, Z., He, P., Li, Y., Ma, J., Chen, W., Zhang, Y., Zhou, X., et al. (2013). Mlkl knockout mice demonstrate the indispensable role of Mlkl in necroptosis. Cell Res. *23*, 994–1006.

Wu, X.N., Yang, Z.H., Wang, X.K., Zhang, Y., Wan, H., Song, Y., Chen, X., Shao, J., and Han, J. (2014). Distinct roles of RIP1-RIP3 hetero- and RIP3-RIP3 homo-interaction in mediating necroptosis. Cell Death Differ. *21*, 1709–1720.

Yang, Z., Wang, Y., Zhang, Y., He, X., Zhong, C.Q., Ni, H., Chen, X., Liang, Y., Wu, J., Zhao, S., et al. (2018). RIP3 targets pyruvate dehydrogenase complex to increase aerobic respiration in TNF-induced necroptosis. Nat. Cell Biol. *20*, 186–197.

Zamaraev, A.V., Kopeina, G.S., Prokhorova, E.A., Zhivotovsky, B., and Lavrik, I.N. (2017). Post-translational Modification of Caspases: The Other Side of Apoptosis Regulation. Trends Cell Biol. *27*, 322–339.

Zaru, R., Ronkina, N., Gaestel, M., Arthur, J.S., and Watts, C. (2007). The MAPK-activated kinase Rsk controls an acute Toll-like receptor signaling response in dendritic cells and is activated through two distinct pathways. Nat. Immunol. *8*, 1227–1235.

Zhang, D.W., Shao, J., Lin, J., Zhang, N., Lu, B.J., Lin, S.C., Dong, M.Q., and Han, J. (2009). RIP3, an energy metabolism regulator that switches TNF-induced cell death from apoptosis to necrosis. Science *325*, 332–336.

Zhang, H., Zhou, X., McQuade, T., Li, J., Chan, F.K., and Zhang, J. (2011). Functional complementation between FADD and RIP1 in embryos and lymphocytes. Nature *471*, 373–376.

Zhao, J., Jitkaew, S., Cai, Z., Choksi, S., Li, Q., Luo, J., and Liu, Z.G. (2012). Mixed lineage kinase domain-like is a key receptor interacting protein 3 downstream component of TNF-induced necrosis. Proc. Natl. Acad. Sci. USA *109*, 5322–5327.

Zhong, C., Yin, Q., Xie, Z., Bai, M., Dong, R., Tang, W., Xing, Y.H., Zhang, H., Yang, S., Chen, L.L., et al. (2015). CRISPR-Cas9-Mediated Genetic Screening in Mice with Haploid Embryonic Stem Cells Carrying a Guide RNA Library. Cell Stem Cell *17*, 221–232.

Please cite this article in press as: Yang et al., A Non-canonical PDK1-RSK Signal Diminishes Pro-caspase-8-Mediated Necroptosis Blockade, Molecular Cell (2020), https://doi.org/10.1016/j.molcel.2020.09.004

STAR★METHODS

KEY RESOURCES TABLE

REAGENT or RESOURCE	SOURCE	IDENTIFIER
Antibodies		
Rabbit anti-caspase-3	Cell Signaling Technology	Cat# 9662; RRID: AB_331439
Rabbit anti-cleaved-caspase-3 (p19 & 17)	Cell Signaling Technology	Cat# 9661; RRID: AB_2341188
Rabbit anti-PARP	Cell Signaling Technology	Cat# 9542; RRID: AB_2160739
Rabbit anti-RSK1	Cell Signaling Technology	Cat# 8408; RRID: AB_10828594
Rabbit anti-RSK2	Cell Signaling Technology	Cat# 5528; RRID: AB_10860075
Rabbit anti-phospho-RSK (S380)	Cell Signaling Technology	Cat# 11989; RRID: AB_2687613
Rabbit anti-phospho-RSK2 (S227)	Cell Signaling Technology	Cat# 3556; RRID: AB_2181465
Rabbit anti-phospho-GSK3β (S9)	Cell Signaling Technology	Cat# 9336; RRID: AB_331405
Rabbit anti-IκBα	Cell Signaling Technology	Cat# 9242; RRID: AB_331623
Rabbit anti-phospho-ERK	Cell Signaling Technology	Cat# 9101; RRID: AB_331646
Rabbit anti-Flag	Cell Signaling Technology	Cat# 14793; RRID: AB_2572291
Rabbit anti-RIP1	Cell Signaling Technology	Cat# 3493; RRID: AB_2305314
Rabbit anti-caspase-8	Cell Signaling Technology	Cat# 4790; RRID: AB_10545768
Rabbit anti-cleaved-caspase-8 (p43 & p18)	Cell Signaling Technology	Cat# 9429; RRID: AB_2068300
Mouse anti-ERK	Cell Signaling Technology	Cat# 9107; RRID: AB_10695739
Rabbit anti-PDK1	Proteintech	Cat# 17086-1-AP; RRID: AB_2161289
Mouse anti-RIP1	BD Biosciences	Cat# 610459; RRID: AB_397832
Mouse anti-Flag (M2)	Sigma-Aldrich	Cat# F3165; RRID: AB_259529
Rabbit anti-HA (Y-11)	Santa Cruz Biotechnology	Cat# sc-805; RRID: AB_631618
Rabbit anti-Myc (A-14)	Santa Cruz Biotechnology	Cat# sc-789; RRID: AB_631274
Mouse anti-GAPDH (6C5)	Santa Cruz Biotechnology	Cat# sc-32233; RRID: AB_627679
Mouse anti-tubulin	Santa Cruz Biotechnology	Cat# sc-32293; RRID: AB_628412
Mouse anti-β-actin (C4)	Santa Cruz Biotechnology	Cat# sc-47778; RRID: AB_626632
Mouse anti-phospho-RIP3 (2D7) (T231, S232)	Abcam	Cat# ab205421
Rabbit anti-phospho-RIP3 (T231, S232)	Abcam	Cat# ab222320
Rabbit anti-phospho-MLKL (S345)	Abcam	Cat# ab196436; RRID: AB_2687465
Rat anti-PECAM (CD31)	BD Biosciences	Cat# 550274; RRID: AB_393571
Alexa Fluor 488 goat anti-mouse antibody	Invitrogen	Cat# A11029; RRID: AB_2534088
Alexa Fluor 594 goat anti-rat antibody	Invitrogen	Cat# A11007; RRID: AB_1056152
Rabbit anti-RIP3	Chen et al., 2013	N/A
Rabbit anti-phospho-RIP3 (T231, S232)	Chen et al., 2013	N/A
Rabbit anti-MLKL	Chen et al., 2013	N/A
Rabbit polyclonal antibody against T265 phosphorylated caspase-8	This paper	N/A
ASC (D2W8U) Rabbit mAb (Mouse Specific)	Cell Signaling Technology	Cat# 67824; RRID: AB_2799736
Chemicals, Peptides, and Recombinant Proteins		
Z-VAD-FMK	Calbiochem	627610
Smac mimetic (SM-164)	APExBIO	A8815
Cycloheximide (CHX)	Sigma-Aldrich	C7698
Propidium iodide (PI)	Sigma-Aldrich	P4170
Necrostatin-1 (Nec-1)	EMD Chemicals	480065
Lipopolysaccharide (LPS)	Sigma	L4524
BI-D1870	MCE	HY-10510

(*Continued on next page*)

Please cite this article in press as: Yang et al., A Non-canonical PDK1-RSK Signal Diminishes Pro-caspase-8-Mediated Necroptosis Blockade, Molecular Cell (2020), https://doi.org/10.1016/j.molcel.2020.09.004

Continued

REAGENT or RESOURCE	SOURCE	IDENTIFIER
SL0101	MCE	HY-15237
FMK	MCE	HY-52101A
Caspase-3/7 Inhibitor I	APExBIO	A1925
SB203580	Calbiochem	559389
BIRB796	Axon Medchem	Axon 1358
PD98059	Sigma	P215
SP600125	Sigma	S5567
GSK470	Selleckchem	S7087
DSS	Pierce	21555
Murine TNFα	Thermo Fisher	PMC3015
Murine EGF	R&D	2028-EG-200
Human EGF	Thermo Fisher	PHG0311
Lambda Protein Phosphatase	NEB	P0753S
DAPI	Sigma-Aldrich	D9542
Polybrene	Sigma-Aldrich	H9268
pLV-H1-EF1α	Biosettia	SORT-B22
Critical Commercial Assays		
CellTiter-Glo® Luminescent Cell Viability Assay	Promega	G7571
Caspase-Glo® 8 Assay	Promega	G8202
Caspase-Glo® 3/7 Assay	Promega	G8092
Deposited Data		
Original data in Mendeley Data	This paper	http://dx.doi.org/10.17632/9phzkmbv9y.2
Experimental Models: Cell Lines		
Mouse: L929 cells	Zhang et al., 2009	N/A
Human: (HEK) 293T	ATCC	CRL-3216
Mouse: Mouse embryonic fibroblasts (MEFs)	This paper	N/A
Mouse: NIH 3T3	Zhang et al., 2009	N/A
Mouse: Raw 264.7	ATCC	TIB-71
Experimental Models: Organisms/Strains		
C57BL/6J mice	Jackson Laboratory	000664
Rip3$^{-/-}$ mice	Wu et al., 2013	N/A
Mlkl$^{-/-}$ mice	Wu et al., 2013	N/A
Casp8$^{+/T265E}$ mice	This paper	N/A
Casp8$^{T265A/T265A}$ mice	This paper	N/A
Casp8$^{+/C362S}$ mice	This paper	N/A
Oligonucleotides		
sgRNA targets *Casp8* for *Casp8*$^{+/T265E}$ and *Casp8*$^{+/T265A}$ mice #1: 5′-AAAGGAACAGACTGTGATAA-3′	This paper	N/A
genotyping primers for *Casp8*$^{+/T265E}$ and *Casp8*$^{+/T265A}$ mice #1: 5′-TCTGCCCTGAAGCTCATCTGTATGG-3′	This paper	N/A
genotyping primers for *Casp8*$^{+/T265E}$ and *Casp8*$^{+/T265A}$ mice #2: 5′-ATGCTTCTCCTTTGGATCCCACCA-3′	This paper	N/A
sgRNA targets *Casp8* for *Casp8*$^{+/C362S}$ mice #1: 5′-GTGTCGTCTATGGAACGGAT-3′	This paper	N/A

(*Continued on next page*)

Please cite this article in press as: Yang et al., A Non-canonical PDK1-RSK Signal Diminishes Pro-caspase-8-Mediated Necroptosis Blockade, Molecular Cell (2020), https://doi.org/10.1016/j.molcel.2020.09.004

Continued

REAGENT or RESOURCE	SOURCE	IDENTIFIER
sgRNA targets *Casp8* for *Casp8*$^{+/C362S}$ mice #2: 5′- GCCCATTAGAAGGTGCTTTA-3′	This paper	N/A
genotyping primers for *Casp8*$^{+/C362S}$ mice #1: 5′-GTGATGCAGAAGGACCGCTCAG-3′	This paper	N/A
genotyping primers for *Casp8*$^{+/C362S}$ mice #2: 5′-GCCCAGGAGGCCAAACTTACTG-3′	This paper	N/A
TALENs′ target sites on mouse *Rip3* were as follows: (Left) 5′-CTAACATTCTGCTGGA-3′; (Right) 5′-TGTAGATGGACTAACC-3′	This paper	N/A
TALENs′ target sites on mouse *Mlkl* were as follows: (Left) 5′-ATCATTGGAATACCGT-3′; (Right) 5′-CTTCCTGCTGCCAGGAT-3′	This paper	N/A
gRNA site of mouse *Rip1* KO: 5′-AACCGCGCTGAGTGAGTTGG-3′	This paper	N/A
gRNA site of mouse *Rsk1* KO: 5′-TGACGTGAACCACCCGTTCG-3′	This paper	N/A
gRNA site of mouse *Rsk2* KO: 5′-TCACCTCCGCGCTGTCGGAA-3′	This paper	N/A
gRNA site of mouse *Casp8* KO: 5′-GCAGGTCCCACCGACTGATG-3′	This paper	N/A
gRNA site of mouse *cFLIP*$_L$ KO: 5′-ACCTGGCTGCACCTAACGTC-3′	This paper	N/A
gRNA site of mouse *Pdk1* KO: 5′-ACTGAGCCCGGTTCGTCCCC-3′	This paper	N/A
shRNA oligos for mouse *Rsk1* #1: 5′-GGACCAAGATGGAGAGAGA-3′	This paper	N/A
shRNA oligos for mouse *Rsk1* #2: 5′-CAGAGGAAATTAAGAGACA-3′	This paper	N/A
shRNA oligos for mouse *Rsk2* #1: 5′-GGAATAATCTATAGAGACT-3′	This paper	N/A
shRNA oligos for mouse *Rsk2* #2: 5′-AGATGGAGTTGAAGAAATT-3′	This paper	N/A
Recombinant DNA		
pBOBI-RIP3 and its mutations	This paper	N/A
pBOBI-Caspase-8 and its mutations	This paper	N/A
pBOBI-RSK1 and its mutations	This paper	N/A
pBOBI-RSK2 and its mutations	This paper	N/A
Software and Algorithms		
GraphPad Prism 6.01	GraphPad	https://www.graphpad.com/scientific-software/prism/
Excel 2016	Microsoft Excel	https://www.microsoft.com/en-us/microsoft-365/excel
BD CellQuest Pro	BD	https://www.bd.com/en-uk/products/molecular-diagnostics/cytometric-analysis-products
ImageJ	NIH	https://imagej.nih.gov/ij/
Image-pro plus 6	Media Cybernetics	https://www.mediacy.com/imageproplus
Aperio ImageScope 64 v12.4.0.5043	Leica	https://www.leicabiosystems.com/cn/digital-pathology/manage/aperio-imagescope/

(*Continued on next page*)

Please cite this article in press as: Yang et al., A Non-canonical PDK1-RSK Signal Diminishes Pro-caspase-8-Mediated Necroptosis Blockade, Molecular Cell (2020), https://doi.org/10.1016/j.molcel.2020.09.004

Continued

REAGENT or RESOURCE	SOURCE	IDENTIFIER
ZEN (blue edition)	ZEISS	https://www.zeiss.com.cn/microscopy/products/microscope-software/zen.html
Other		
Flag-M2 affinity resin	Sigma-Aldrich	A2220
Protease Inhibitor Cocktail	Sigma-Aldrich	S8820
Antigen-coupled CN-Br activated Sepharose 4B	GE	17043001
A/G agarose beads	Thermo Fisher	20422
Rabbit TrueBlot	Thermo Fisher	18-8816-33
FACS Calibur flow cytometer	BD Bioscience	https://www.bdbiosciences.com/en-us
POLAR star Omega	BMG Labtech	https://www.bmglabtech.com/cn/polarstar-omega/

RESOURCE AVAILABILITY

Lead Contact

Further information and requests for resources and reagents should be directed to and will be fulfilled by the Lead Contact, Jiahuai Han (jhan@xmu.edu.cn).

Materials Availability

All materials generated in this study are available on request to Lead Contact.

Data and Code Availability

Original data have been deposited to Mendeley Data: http://dx.doi.org/10.17632/9phzkmbv9y.2.

EXPERIMENTAL MODEL AND SUBJECT DETAILS

Cell Culture

Mouse fibroblast L929 cells (mouse male), mouse Raw 264.7 cells (mouse male) and human embryonic kidney (HEK) 293T (human female) cells were obtained from American Type Culture Collection (ATCC). The A line of NIH 3T3 (mouse male) cells was described previously (Zhang et al., 2009). MEF was generated and infected as described before (Newton et al., 2014). Briefly, All MEFs were from E9.5 or E13.5 embryos and infected with the retroviral Large T, pWZL-hygro-E1A and pWZL-hRAS, respectively. All cells were cultured in Dulbecco's Modified Eagle's Medium (Invitrogen) supplemented with 10% fetal bovine serum (GIBCO), 1% MEM non-essential amino acids solution (Hyclone), 100 units/ml penicillin/streptomycin, at 37°C in a humidified incubator containing 5% CO_2. All cell lines were well established and frequently checked by monitoring morphology and functionalities. All the cell lines were authenticated by STR analysis and were routinely tested to be mycoplasma-free.

Mice

Rip3$^{-/-}$ *and Mlkl*$^{-/-}$ mice were generated by transcription activator-like effector nucleases (TALENs)-mediated gene-disruption method in a C57BL/6 background, as described previously (Wu et al., 2013). Genotypes were confirmed by tail-snip PCR. *Casp8*$^{+/T265E}$, *Casp8*$^{+/T265A}$ and *Casp8*$^{+/C362S}$ mice were generated by CRISPR/Cas9 and haploid embryonic stem cell systems (Zhong et al., 2015). The haploid embryonic stem cell was a kind gift from Jin-Song Li (SIBCB, CAS). For *Casp8*$^{+/T265E}$ and *Casp8*$^{+/T265A}$ mice, genotyping amplified 414 bp DNA fragment. For *Casp8*$^{+/C362S}$ mice, genotyping amplified 615 bp DNA fragment. And the genotyping results were confirmed by sequencing. All knock-in mice were backcross with C57BL/6 at least 8 generations, and mice with H19 and DMR mutations were excluded by using PCR as previously reported (Zhong et al., 2015). Additional information is provided upon request. Sex preference did not exist in the mouse models used here and both male and female mice were used in this study. Littermates of the same sex were randomly assigned to the control or experimental groups. All mice were housed in specific pathogen-free condition with 12-hour light/dark cycle and access to food and water *ad libitum* at the Xiamen University Laboratory Animal Center. All mouse experiments were approved by the Institutional Animal Care and Use Committee and were in strict accordance with good animal practice as defined by the Xiamen University Laboratory Animal Center.

Please cite this article in press as: Yang et al., A Non-canonical PDK1-RSK Signal Diminishes Pro-caspase-8-Mediated Necroptosis Blockade, Molecular Cell (2020), https://doi.org/10.1016/j.molcel.2020.09.004

METHOD DETAILS

SIRS Mouse Model

Mice were housed in a specific pathogen-free environment. All experiments were conducted in compliance with the regulations of Xiamen University Laboratory Animal Center. Six- to eight-week-old sex-matched mice (average weight approximately 20 g) were injected intravenously with 300 μg/kg TNF (75 μg/ml) diluted in endotoxin free PBS. To the BI-D1870 treatment group, BI-D1870 diluted in endotoxin free PBS was injected intravenously with 10 mg/kg 1 hour before TNF injection. Mice injected with DMSO diluted in PBS were included as controls. Animals were under permanent observation and survival was checked every 30 min. Littermates of *Rip3*$^{-/-}$, *Rip3*$^{-/-}$*Casp8*$^{-/-}$ and WT, *Casp8*$^{T265A/T265A}$ and *Casp8*$^{+/+}$ mice were used in the experiments. Mice were sacrificed at indicated time or when body temperature was below 23.6°C. The investigator was blinded to allocation when the mice were injected with TNF and when mice deaths were counted.

Histology

After animals were euthanized, embryos and caecum were collected immediately, and fixed in 4% paraformaldehyde in PBS for 24 hours. The fixed tissues were dehydrated in ethanol, cleared in xylene, and embedded in paraffin blocks. Five-micrometre sections were cut and mounted on adhesion microscope slides (ZSGB-BIO), and then stained with hematoxylin and eosin (H&E), rabbit anti-phospho-MLKL (S345), mouse anti-phospho-RIP3 (2D7), rabbit anti-phospho-Casp8 (T265), rabbit anti-ASC (D2W8U) or rabbit anti-cleaved-Casp3 for analyses. IHC staining was performed as described (Chen et al., 2015). The degree of caecum damage was assessed by a method described previously (Coburn et al., 2005). Representative images were captured and processed using identical settings in the Leica Aperio Versa 200 at Xiamen University. The investigators were blinded to allocation when the histology experiments were performed and tissue damage was scored.

Immunofluorescence Microscopy

Yolk sacs were harvested, mounted on adhesion microscope slides (ZSGB-BIO) and fixed for 2 h using 4% paraformaldehyde in PBS. Cells were permeabilized for 45 min in 0.25% Triton X-100 in PBS, blocked for 1 hour in PBS containing 2% goat serum, and incubated for 2 hours at room temperature with mouse anti-phospho-RIP3 (2D7) along with PECAM (CD31) diluted in blocking buffer. Yolk sacs were washed three times with PBS and then incubated for 1 hour at room temperature with Alexa Fluor 488 goat anti-mouse antibody (A11029, Invitrogen) and Alexa Fluor 594 goat anti-rat antibody. DAPI was used as a nuclear (DNA) counter stain. Images were acquired on a Zeiss LSM 780 laser scanning confocal microscope.

Generation of Knockout Cell Lines

Rip3 knockout (KO) and *Mlkl* KO L929 cell lines were generated using TALE-nuclease (TALENs) methods. *Rip1* KO, *Rsk1* KO, *Rsk2* KO, *Casp8* KO, *cFLIP*$_L$ KO and *Pdk1* KO L929 cell lines were generated using CRISPR/Cas methods. The disruption of target gene was determined by the sequencing of gene loci and by the immunoblotting of cell lysates with antibodies.

Lentivirus Production and Infection

HEK293T cells were transfected with lentiviral vectors carrying cDNAs or shRNAs of interest (or its mutants) and lentivirus-packing plasmids (PMDL/REV/VSVG) by the calcium phosphate precipitation method. 12 hours later, cell culture medium was changed and the virus-containing medium was collected 36 h later. For infection, virus containing medium in the presence of 10 μg/ml Polybrene was added to cells plated in 12-well plates and then centrifuged at 2,500 rpm for 30 min. The medium was changed 12 h later. For RNA interference, shRNAs were expressed using a lentiviral vector pLV-H1-EF1α. The control shRNA was as described (Zhang et al., 2009). The sequence of shRNA oligos for mouse *Rsk1* and *Rsk2*. RSK1 shRNA-resistant expression constructs were generated by mutation on shRNA targeting site at 6 different bases without changing amino acid sequence.

Immunoblotting and Immunoprecipitation

Cell pellets were collected in ice-cold PBS and re-suspended in lysis buffer (20 mM Tris-HCl, pH7.5, 150 mM NaCl, 1 mM Na_2EDTA, 1 mM EGTA, 1% Triton X-100, 2.5 mM sodium pyrophosphate, 1 mM β-glycerophosphate, 1 mM Na_3VO_4 and Protease Inhibitor Cocktail. The re-suspended cell pellets were sonicated and centrifuged at 20,000 x *g* for 30 min at 4°C. The supernatants were collected for immunoblotting or immunoprecipitation. Commercially available anti-Flag beads were used in the immunoprecipitation. For immunoprecipitation of endogenous proteins, antibody coupled beads were made as follows. Antibodies were purified from serum using antigen-coupled CN-Br activated Sepharose 4B and were then crosslinked to A/G agarose beads with DSS at room temperature for 1 hour. The cell lysates were then incubated with the antibody-coupled beads overnight at 4°C. The beads were washed with lysis buffer and the immunoprecipitates were eluted off the beads with 125 mM Glycine (pH2.5). The acid eluents were neutralized by adding 1/10 volume of 1M Tris-HCl (pH8.0) and subjected to immunoblotting. To minimize the influence of IgG in immunoblotting, the Rabbit TrueBlot was used.

Please cite this article in press as: Yang et al., A Non-canonical PDK1-RSK Signal Diminishes Pro-caspase-8-Mediated Necroptosis Blockade, Molecular Cell (2020), https://doi.org/10.1016/j.molcel.2020.09.004

Mass Spectrometry Analysis

Flag-caspase-8 was immunoprecipitated using anti-Flag M2 beads from cell lysates followed by SDS-PAGE. The caspase-8 band was excised from Coomassie-stained gels and subjected to in-gel digestion. Briefly, gel fragments were destained with 50% acetonitrile/50mM ammonium bicarbonate followed with incubation in 10 mM DTT at 56°C for 30min for cysteine reduction, and cysteines were alkylated with 50 mM iodoacetamide for 30 min at RT in darkness. Trypsin was then added at the ratio of protein: trypsin = 50:1 and digestion was carried out at 37°C for 12 hours. Tryptic peptides were extracted from gels using 0.15% formic acid/67% acetonitrile and dried prior to phosphopeptide enrichment. Phosphopeptides were enriched using immobilized metal ion affinity chromatography (IMAC). Dried Peptides were dissolved in 0.1% formic acid/2% acetonitrile and separated on a fused silica capillary emitter (75μm inner diameter) packed in-house with 5 μm C18 resin (New Objective), and analyzed on AB SCIEX TripleTOF 5600 system. For information dependent acquisition (IDA), survey scans were acquired in 250ms and 20 product ion scans were collected in 50ms/per scan. The acquired raw data files (.wiff) were searched with ProteinPilot software V.4.2 against caspase-8 protein sequence database with common contaminants included. The following search parameters were selected: sample type (identification), cys alkylation (iodoacetamide), digestion (trypsin), instrument (TripleTOF 5600), special factors (phosphorylation emphasis), and search effort (thorough). The tolerances were specified as ± 0.05 Da for peptides and ± 0.05 Da for MS/MS fragments.

Cell Death Assay

Cell death was analyzed using FACS or CellTiter-Glo Luminescent Cell Viability Assays kit. FACS analysis was performed as previously described (Zhang et al., 2009). In brief, cells were trypsinized, resuspended with PBS containing 5 μg/ml Propidium iodide (PI) and quantified on a FACS Calibur flow cytometer. PI-negative cells with normal size were considered as living cells. The Luminescent Cell Viability Assays were performed according to the manufactory′s instructions. In brief, 1.0×10^5 cells were seeded in 96-well plates with white wall. After treatment, equal volume of CellTiter-Glo reagent was added to the cell culture medium, which had been equilibrated to room temperature for 30 min. Cells were shaken for 5 min and incubated at room temperature for 15 min. Luminescent recording was performed with POLAR star Omega (BMG Labtech, Durham, NC, USA).

Caspase-8 Activity Assay

Caspase-8 activity was determined by using a Caspase-Glo 8 assay kit according to the manufacturer′s instructions. In brief, 1.0×10^5 cells were seeded in 96-well plates with white wall. After treatment, equal volume of Caspase-Glo 8 reagent was added to the cell culture medium, which had been equilibrated to room temperature for 30 min. Cells were shaken for 5 min and incubated at room temperature for 30 min. Luminescent recording was performed with POLAR star Omega (BMG Labtech, Durham, NC, USA).

Kinase Activity Assay

The anti-RSK1 immunoprecipitates were washed three times with kinase buffer (50 mM HEPES [pH 7.5], 10 mM $MgCl_2$, 50 mM NaCl, 0.02% BSA, 150 mM ATP, and 1 mM DTT), and then incubated at 37°C for 1 hour with GST-GSK3β and ^{32}P-ATP as described (Yang et al., 2018). The reaction mixtures were then subjected to SDS-PAGE.

QUANTIFICATION AND STATISTICAL ANALYSIS

Data were presented as the mean ± SD of triplicates. Data were analyzed and presented with GraphPad Prism 6.01 software. The statistical significance of the differences between the two groups was determined by the Student′s t test. Mice survival was presented as a Kaplan–Meyer plot and compared by log-rank (Mantel–Cox) Test. To evaluate the caecum damage between the two genotypes or two groups, a Wilcoxon signed-rank test was performed. Differences in compared groups were considered statistically significantly different with P values: ns: $p \geq 0.0.5$; *: $p < 0.05$; **: $p < 0.01$; ***: $p < 0.001$;****: $p < 0.0001$.